Modal Decomposition of the Velocity Field near the Oregon Coast

Pijush K. Kundu, J. S. Allen and Robert L. Smith

School of Oceanography, Oregon State University, Corvallis 97331

(Manuscript received 9 December 1974, in revised form 7 May 1975)

ABSTRACT

The low-frequency [$\omega < 0.5$ cycle per day (cpd)] current fluctuations at four depths in 100 m of water have been investigated for two stations on the continental shelf off the coast of Oregon. One station, DB-7, was maintained during the summer of 1972 as part of the Coastal Upwelling Experiment-1 (CUE-I), and the other station, Carnation, was maintained during the summer of 1973 as part of CUE-II. A decomposition of the north–south (almost alongshore) v and the east–west (onshore–offshore) u components of the current has been performed in terms of two types of modal structures in the vertical direction: (i) dynamic modes determined by the separable solutions of the appropriate equations of motion, and (ii) empirical orthogonal modes which are the eigenvectors of the correlation matrix and depend only on the statistics of the data. For the alongshore currents, the standard deviation of the dynamic barotropic mode is found to be twice as large as that of the first baroclinic mode. The barotropic part is found to be correlated with the north–south component of the wind stress τ_W and the sea level, whereas the first mode baroclinic part is found to be correlated with the temperature fluctuations. The first empirical eigenmode accounts for about 91% of the energy and is fairly depth-independent, whereas the second empirical eigenmode accounts for about 7% of the energy and resembles the first dynamic baroclinic mode. Spectral analysis shows high mutal coherence between the barotropic modes for the u and v components and the wind stress τ_W at the frequencies 0.06 cpd in 1973 and 0.14 cpd in 1972. Results from a theoretical model show that the observed values of the phase relations at these frequencies are consistent with a resonant condition between the wind stress and forced, long, barotropic continental shelf waves.

1. Introduction

The occurrence of coastal upwelling off the coast of Oregon due to the predominantly southward wind during the summer months is well known. Continuous velocity measurements were made at several stations on the continental shelf during the Coastal Upwelling experiments, CUE-I in 1972 and CUE-II in 1973. Based on the experimental data taken during the summer of 1972 as part of CUE-I, Smith (1974) has given a detailed description of the phenomenon and pointed out some interesting features of the low-frequency variations in the current at one station, DB-7, and their relationship with the wind and the sea level fluctuations. The existence of a strong depth-independent, or barotropic, component in the alongshore velocities is evident from the results.

In order to formally separate the barotropic and baroclinic components of the velocity field, it was decided to decompose the velocity field in the vertical direction into its modal components. This was felt to be especially important since theoretical results (see Appendix A) indicate that there should be a large baroclinic response which is limited to a region with an offshore scale of the order of the internal Rossby radius of deformation ($\sim$15 km) and hydrographic data (e.g., Mooers *et al.*, 1972; Smith, 1974) have tended to support that picture.

In this paper, the modal decomposition has been applied to the velocity measurements from DB-7 and to measurements from an analogous station, Carnation, which was maintained during CUE-II. This enables some of the features of the CUE-II observations to be studied and the results from measurements at similar stations in two different years to be compared. The objectives of the present work are, therefore, twofold:

1) To decompose the velocity field into its modal components and determine the relative strengths of the various modes as well as their relationship with the wind, sea level and temperature. Both dynamic modes, determined by the separable solutions of the appropriate equations of motion, and "empirical orthogonal modes," determined by the statistics of the data, are used.

2) To present some simple dynamical arguments in an attempt to explain some of the observed features of the data.

The outline of the paper is as follows. The observations are described in Section 2. The hydrography is given in Section 3 and some basic features of the currents, wind and sea level are discussed in Section 4. The currents are decomposed into dynamic modes in Section 5 and into empirical orthogonal modes in Section 6. In Section 7, the relation of the dynamical

and empirical modes with the wind stress, sea level and temperature is described. A dynamical discussion of the data is given in Section 8 and the paper is summarized in Section 9. In Appendix A, the relevant theoretical considerations are presented while Appendix B contains an interpretation of the empirical orthogonal decomposition.

2. The observations

The previous paper by Smith (1974) was based on the current measurements at four depths (20, 40, 60 and 80 m below the surface) in 100 m of water at the current meter station DB-7 (Fig. 1) for 48 days from 10 July to 26 August, 1972. The basic current meter array for CUE-II was placed approximately 60 km north of that of CUE-I to take advantage of the simpler bathymetry in that region. One mooring of the CUE-II current meter array, called Carnation (Fig. 1), was very similar to DB-7 in the sense that current and temperature measurements were taken at 20, 40, 60, 80 and 95 m in 100 m of water for 54 days from 3 July to 25 August 1973. This similarity of the two stations allows a comparison of the results for two different upwelling seasons.

The currents and temperatures were measured with Aanderaa current meters suspended beneath subsurface

FIG. 1. The region of the observational study off Oregon. Bathymetric contours are in meters.

floats at 15 m. The Aanderaa current meters recorded speed, direction and temperature at 5 or 10 min intervals. The acquisition and processing of the time series data from the moored buoys in CUE-I and CUE-II are described by Pillsbury et al. (1974). This included filtering of the 5 or 10 min observations to obtain hourly time series. The hourly data sets were then filtered, in a manner identical to that used by Smith (1974), to eliminate the tidal and inertial oscillations by means of a symmetrical filter spanning 121 h with a half-power point of 40 h (half-amplitude at 0.7 cpd, half-power at 0.6 cpd, 90% power at 0.5 cpd). The resulting series was then decimated to 6-hourly values. In 1972 the wind and atmospheric pressure were measured at Newport, whereas the sea level was measured by a tide gauge at Depoe Bay. In 1973 the wind, the atmospheric pressure, as well as the sea level were measured at Newport.

3. Hydrography

The density (sigma-t) section for late June 1973, shown in Fig. 2, is typical for the upwelling season off Oregon and is qualitatively similar to the sections observed in June 1972. Over the continental slope and shelf the isopleths of temperature, salinity and density slope upward toward the coast from May to October. In contrast, from late fall to early spring the isopycnals are essentially level and deeper, e.g., the 26.0 isopycnal intersects the shelf between 100 and 150 m. The shear in the alongshore currents predicted from the density sections, using the "thermal wind" equation, has been found in previous studies of the CUE-I data to be in close agreement with that obtained from the low-frequency current meter data at the time of the section (Smith, 1974; Huyer et al., 1974).

The density distribution varies little during June, July and August despite fluctuations in the wind, except above 20 m or within 10 km of the coast where the density field responds appreciably and rapidly to variations in the wind on the time scale of days to a week. This can be seen by comparing the sigma-t sections for 10 July and 13 July 1973. The wind had been weakly northward during early July and the 10 July section shows the warm, low-salinity water ($\sigma_t < 24.5$) of the Columbia River plume covering the coastal region. The wind became strongly southward on 10 July and a strong offshore Ekman transport presumably developed. By 13 July the Columbia River plume had been swept offshore.

The current meter arrays (DB-7 in 1972 and Carnation in 1973) were located about 13 km from the coast, which appears to be just offshore of the zone which experiences very large fluctuations in the density with wind variations. The uppermost current meter (20 m below the surface) was just at the bottom of the surface layer which experiences much larger variations than the rest of the water column.
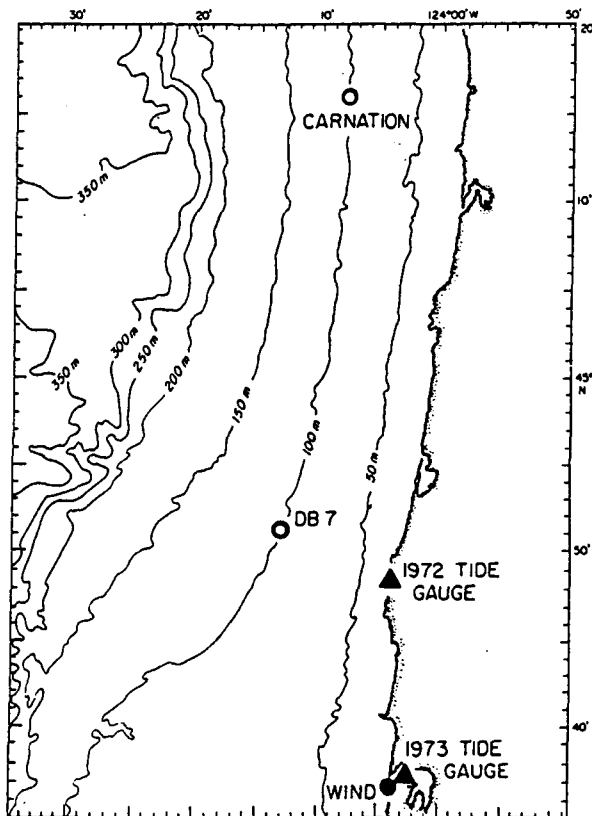
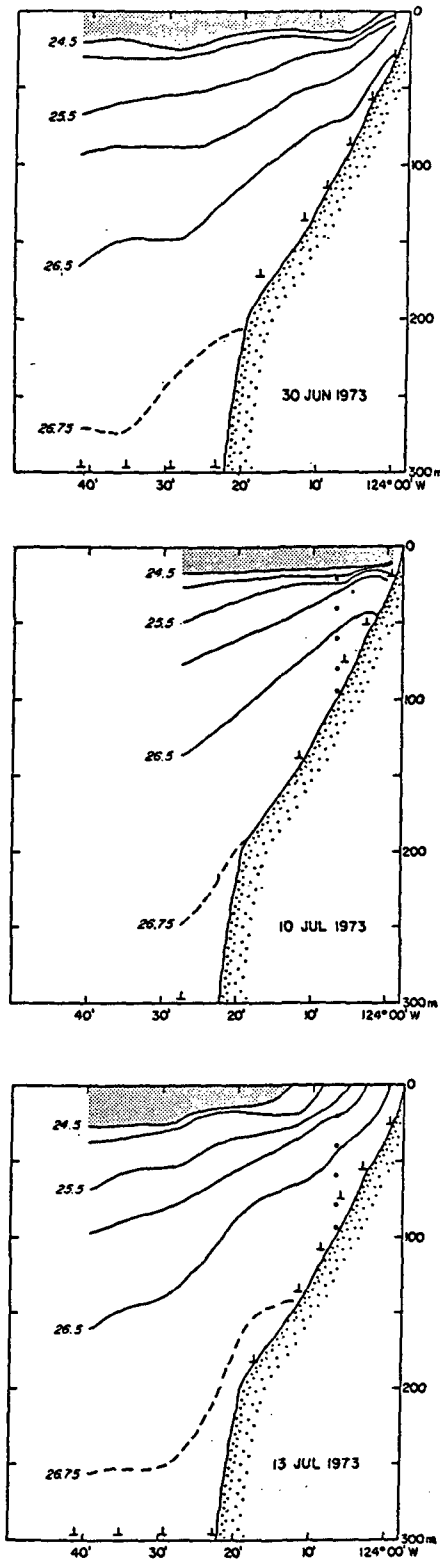FIG. 2. Vertical sections of sigma-t along 45°61'N during June–July 1973. The position of the current meters at Carnation are indicated by solid dots. Contour intervals (0.5 sigma-t units for sigma-t >24.5) are not shown for shaded area (sigma-t <24.5). Station positions are marked by inverted tees.

4. Description of the currents, wind and sea level

All quantities will be referred to a Cartesian coordinate system (x, y, z) with x positive eastward, y positive northward, and z positive upward, with the origin placed at the coast. The time mean of a variable will be denoted by an overbar, and its time fluctuations will be induced by a prime. The eastward, northward and upward velocities will be denoted by u, v and w, respectively, so that at point x the eastward velocity is

$$u(\mathbf{x},t) = \bar{u}(\mathbf{x}) + u'(\mathbf{x},t).$$

The normalized lagged correlation function between the fluctuating parts of two quantities q_1 and q_2 is defined as (assuming stationarity)

$$r_{12}(\tau) = \frac{\overline{q_1'(t)q_2'(t+\tau)}}{(\overline{q_1'^2})^{\frac{1}{2}}(\overline{q_2'^2})^{\frac{1}{2}}}.$$

The zero-lag correlation $r_{12}(0)$ will simply be referred to as the correlation coefficient.

FIG. 3 shows the north–south components of the wind and currents, as well as the barometrically adjusted sea level for 1973 data, and Fig. 4 shows the same for 1972, reproduced from Smith (1974) for the
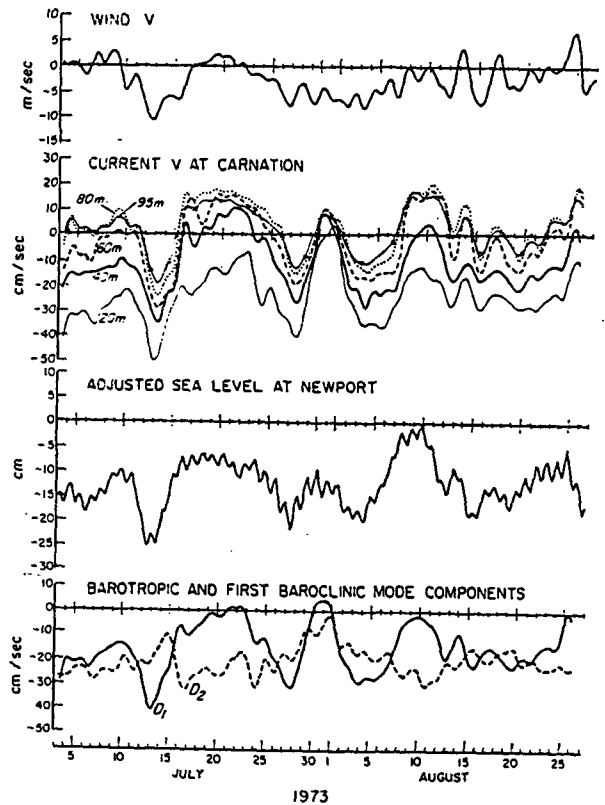

FIG. 3. North–south component of wind and currents, and adjusted sea level, for 1973. The bottom curves (D_1 and D_2) are the amplitudes of barotropic and first baroclinic components.
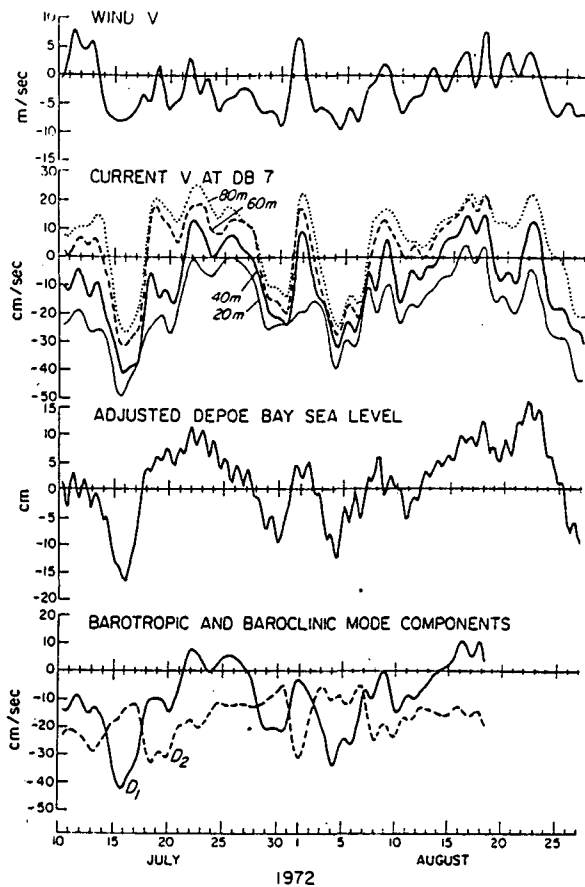
FIG. 4. As in Fig. 3 except for 1972.

panied by a depression of the sea level at the coast, which is consistent with an alongshore barotropic current in geostrophic balance.

The east-west components of the currents from Carnation are plotted, along with the barotropic and first baroclinic modes, in Fig. 5. It can be seen that, aside from the fact that there appears to be a mean onshore flow at all depths over the total time period, the picture presented by these components is a great deal more complicated than that by the alongshore velocities. While the currents at 20, 40, 60 and 80 m are sometimes ordered in magnitude, with the 20 m being the largest and the 80 m the smallest (see the time period 18 July–1 August), there are many instances where the 20 m current violates this pattern. It is possible that at times the mixed layer deepens and affects the 20 m onshore–offshore current, resulting, for example, in an offshore "Ekman-like" flow at 20 m while an onshore flow prevails at other depths.

Some basic statistics of the wind, the barometrically adjusted sea level, and the currents at DB-7 and Carnation are compared in Table 1. The standard errors ($\pm\epsilon$) of the mean, calculated according to Kundu and Allen (1975), are included. The standard deviation of v' remains virtually constant with depth, whereas that of u' shows a slow decrease with depth. This may be due to the east-west slope of the bottom, which allows a north-south excursion of the fluid particles but obstructs their east-west excursion. The 95 m current at Carnation shows the frictional effects of the bottom (at 100 m depth) in terms of the lower mean and rms velocities.

sake of comparison. The bottom curves on both Figs. 3 and 4 are the time series of the barotropic and the first-mode baroclinic parts of the currents, as explained in Section 5. From the nature of the variations of the currents at different depths, a large part of the alongshore current variations appears to be depth-independent, or barotropic,[1] with a vertical shear which is not greatly variable in time. Note, also, that a strong, sustained southward wind generally produces a southward current at all depths. However, there are also exceptions; for example, the large current changes at all depths in Carnation during 28 July–3 August are apparently not related to wind changes. Note, also, that a southward current variation is very closely accompanied

[1] A little caution is needed here. For example, suppose there is a strong first baroclinic mode present in the ocean, with no barotropic mode. If all the measurements are taken below the node, then the resulting series may give a spurious impression of barotropy. This indicates why a simple depth average of data inadequately sampled in the vertical is not a valid way of finding the barotropic part. To decompose the motion into its barotropic and baroclinic components, the modal shapes (and hence the density structure which determines these shapes) must be known. This is done in Section 5.
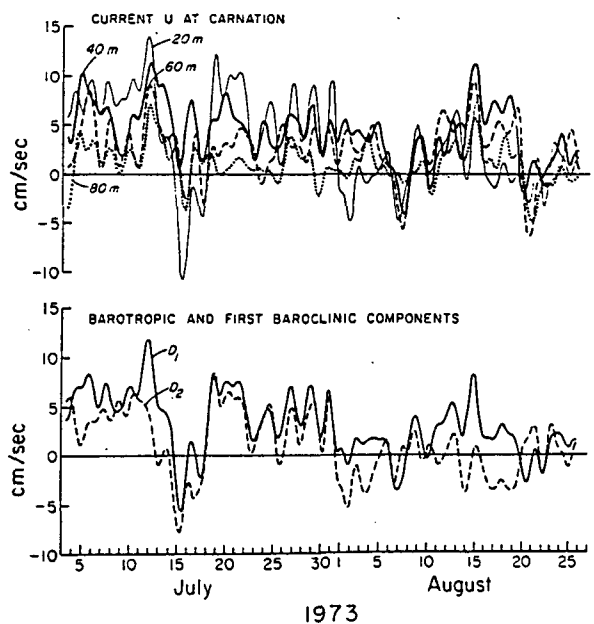

FIG. 5. East-west component of currents at Carnation and their barotropic and first baroclinic amplitudes.

TABLE 1. Comparison of basic statistics for 1972 and 1973.

	U Mean		U S.D.		V Mean		V S.D.	
	72	73	72	73	72	73	72	73
Wind (m s^{-1})	0.7±0.4	0.6±0.2	1.2	0.5	−2.2±1.3	−2.5±1.1	4.2	3.5
20 m current (cm s^{-1})	−3.4±1.6	3.2±1.5	5.2	4.7	−18.1±3.8	−23.9±3.2	12.0	10.0
40 m current (cm s^{-1})	0.4±1.9	4.3±0.9	6.0	3.0	−7.9±4.2	−10.9±3.3	13.4	10.5
60 m current (cm s^{-1})	2.6±1.5	2.7±0.9	4.9	2.9	1.6±4.6	−2.0±3.7	14.5	11.7
80 m current (cm s^{-1})	3.1±1.3	1.1±6.3	4.1	2.0	6.1±4.4	2.9±3.4	13.8	10.7
95 m current (cm s^{-1})		0.6±0.5		1.7		2.5±2.7		8.4
Sea level (cm)					S.D. (72)=6.4 S.D. (73)=4.8			

1. 1972 samples are twice daily values for 48 days, from 1200 GMT 10 July to 1200 GMT 26 August 1972, with the exception of the 60 m current which runs only up to 18 August.

2. 1973 samples are twice daily values for 54 days, from 1200 GMT 3 July to 1200 GMT 25 August.

5. Decomposition into dynamic modes

To further investigate the nature of the fluctuations occurring in the currents, it is advantageous to separate the motion into its barotropic (depth-independent) and baroclinic components. It is shown in Appendix A that the solution for the pressure of the appropriate simplified equations of motion can be written as a sum of modes:

$$p = \sum_{n=1}^{\infty} Y_n(y,t) X_n(x) Z_n(z), \qquad (5.1)$$

where X_n is given by

$$X_n = \exp(\gamma_n x), \qquad (5.2)$$

and Z_n satisfies

$$\left[\frac{f^2 Z_{nz}}{N^2(z)}\right]_z + \gamma_n^2 Z_n = 0. \qquad (5.3)$$

Here $N(z)$ is the Brunt-Väisälä frequency, f the Coriolis parameter, the subscript z denotes the z derivative, and γ_n is the eigenvalue. The mode shapes in z are solutions of the eigenvalue problem defined by (5.3) with homogeneous boundary conditions

$$Z_{nz} = 0, \quad z = 0, H, \qquad (5.4)$$

which follows from the assumption of a flat bottom (see Appendix A).

Because of the assumed geostrophy of the alongshore velocity, $v = -p_x/(\rho_0 f)$, v may be written, using

(5.1), as

$$v(z,t) = \sum_{n=1}^{\infty} D_n(t) Z_n(z), \qquad (5.5)$$

where $D_n = \gamma_n Y_n X_n/(\rho_0 f)$ and the dependence on (x,y) has been suppressed. It can be shown from the nature of the present eigenvalue problem that the eigenfunctions are orthogonal with respect to a weighting function of unity.

It is advantageous to normalize each eigenfunction such that

$$\frac{1}{H} \int_0^H Z_n Z_m dz = \delta_{nm}, \qquad (5.6)$$

where δ_{nm} is the Kronecker delta, so that

$$\frac{1}{H} \int_0^H v^2 dz = \sum_{n=1}^{\infty} D_n^2, \qquad (5.7)$$

which is the Parseval identity. That is, the square of each D_n gives the instantaneous contribution of a particular mode to the depth-integrated energy at a certain station. Comparison of the rms values of the time series of the various $D_n(t)$ then determines the relative strengths of the different modes.

Mode shapes for the Oregon coast region were found by solving the eigenvalue problem defined by (5.3) and (5.4), with hydrographic data used to compute $N(z)$. For Carnation, the data were taken from the measurements of Holbrook and Halpern (1974), who had an

anchor station at this position and reported a total of 193 instantaneous vertical profiles of the Brunt-Väisälä frequency during July–August of 1973. A smoothed average over these 193 profiles was taken to represent $N(z)$. For the station DB-7, the data were from the measurements of Halpern and Holbrook (1972), taken during the July–August of 1972. A total of seven σ_t profiles, taken within about 4 km of DB-7, were averaged, and $N(z)$ was estimated from this through a numerical differentiation scheme using a 5-point least-square parabola. The resulting $N(z)$ for the two stations are shown in Fig. 6. The two $N(z)$ profiles, representing different years' data, are seen to be somewhat similar, except that at Carnation the pycnocline (maximum N) is somewhat stronger (N_{max} = 0.5 cpm) and shallower (8 m deep) compared to DB-7 (N_{max} = 0.37 cpm at 13 m).

The mode shapes were computed by integrating (5.3) by means of a fourth-order Runge-Kutta technique, with a trial-and-error procedure for determining the proper values for γ_n so that the boundary conditions (5.4) were satisfied. The first four baroclinic eigenvalues for the two stations are given in Table 2. The eigenvalue $\gamma_1 = 0.0$, of course, represents the barotropic mode, Z_1 = constant and X_1 = constant, which is just the nearshore approximation for the barotropic motion which varies on a larger x-scale (see Appendix A). From (5.2) it is apparent that the higher baroclinic modes decay in the offshore direction faster than the lower modes. The lowest baroclinic mode decays to $\exp(-3.0) \approx 0.05$ times its value at the coast in an offshore distance of

$$\delta x = 3.0/\gamma_2 \approx 16 \text{ km}$$

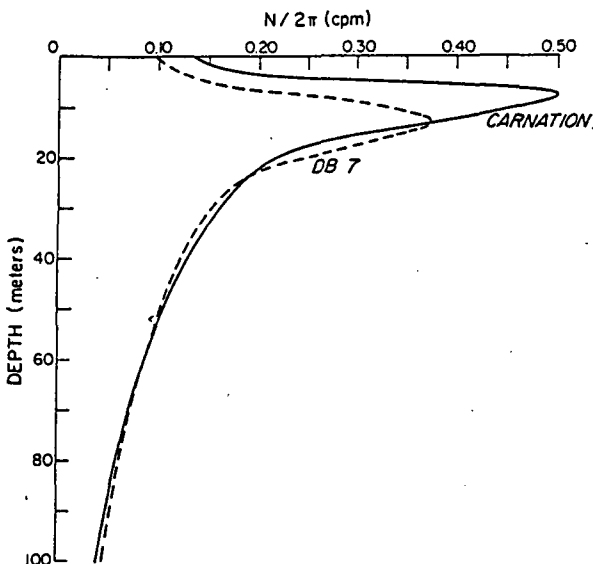for both stations. We call this distance the effective

FIG. 6. Vertical profiles of the Brunt-Väisälä frequency.

TABLE 2. Dynamic eigenvalues (km^{-1}).

Carnation	DB-7
$\gamma_2 = 0.18$	$\gamma_2 = 0.18$
$\gamma_3 = 0.38$	$\gamma_3 = 0.42$
$\gamma_4 = 0.61$	$\gamma_4 = 0.67$
$\gamma_5 = 0.82$	$\gamma_5 = 0.90$

internal Rossby radius of deformation for the Oregon coast.

The first four modes calculated for Carnation are shown in Fig. 7, all of which are normalized according to (5.6). The modes for DB-7 are similar and are not shown.

Having determined the mode shapes, the next step is to fit them to the data so as to determine the relative strengths of the barotropic and baroclinic parts of the currents. It should be noted that, although the modes $Z_n(z)$ are orthogonal in the continuous sense (5.6), they do not necessarily satisfy a discrete analog of (5.6); i.e., it is found that

$$\sum_{j=1}^{J} Z_n(z_j)Z_m(z_j) \neq \delta_{mn}, \qquad (5.8)$$

where z_j are specified by the sampling depths. The orthogonality properties of the Z_n, therefore, may not be used directly to determine the coefficients D_n. We have chosen to determine the D_n by least-square fitting the data with the computed mode shapes, that is, choosing the various D_n such that the error

$$\sum_{j=1}^{J} [v(z_j,t) - \sum_{n=1}^{N} D_n(t)Z_n(z_j)]^2 \qquad (5.9)$$

is minimum. This leads to a set of simultaneous linear algebraic equations in the D_n. At both Carnation and DB-7, currents at 20, 40, 60 and 80 m were used ($J = 4$); the 95 m current at Carnation was ignored because it displayed frictional effects of the bottom. Although the modal amplitudes $D_n(t)$ were determined with the time mean kept in the data series, removing the mean would have only resulted in $\bar{D}_n(t) = 0$ with the time fluctuations $D_n'(t)$ unchanged, both for an exact or a least-square fit.

Only the first (barotropic) and the second (first baroclinic) modes have been used in the least-square fitting (5.9). The third mode could not be accurately fitted since in the present case the discretely sampled third mode is very similar to a linear combination of the discretely sampled first and second modes, as is evident from Fig. 7 for Carnation. If the data has energy in these higher modes, this will be reflected in the lower mode amplitudes ("aliasing"). However, the higher modes decay offshore faster than the lower modes. In fact, from (5.2), if the second and third mode amplitudes are equal at the coast, then at a distance
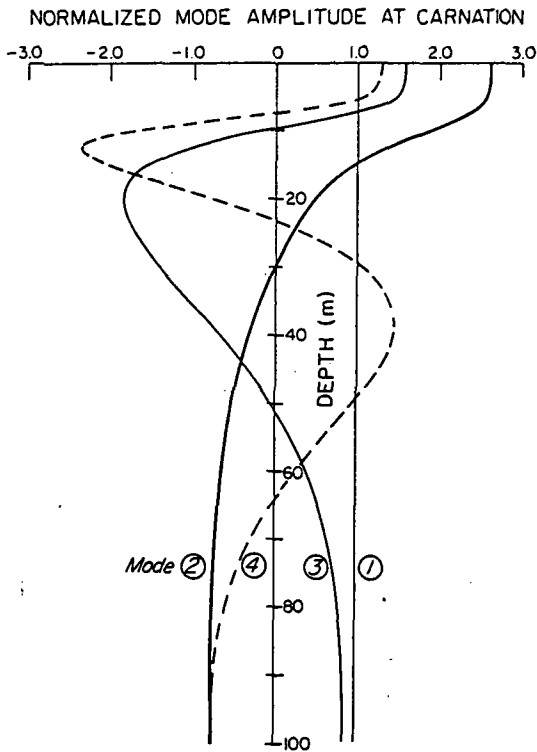
NORMALIZED MODE AMPLITUDE AT CARNATION

FIG. 7. Vertical profiles of first four modes at Carnation.

x from the coast their ratio is $X_3/X_2 = \exp(\gamma_2 - \gamma_3)x$, which for Carnation or DB-7 ($x \approx 10$ km) is about 0.09.[2] The data are therefore expected to contain low values of third and higher mode energy.

The east-west component of the velocity at Carnation was also decomposed into a barotropic and a first baroclinic mode. The mode shapes Z_n for u are the same as those for v, which is easy to see from Eqs. (A2b, c). In spite of the apparent mixed layer influence on the u at 20 m, the 20 m current was retained in the calculation for D_1 and D_2 since it is the only measurement on the surface side of the node of the first baroclinic mode and because it is not clear that it properly should be omitted.

The amplitudes $D_1(t)$ and $D_2(t)$ for the alongshore component, determined by the least-square fitting, are shown as the bottom curves in Fig. 3 for Carnation and Fig. 4 for DB-7; those for the u component for Carnation are shown in Fig. 5. The means, standard deviations and correlations of these modal amplitudes are shown in Table 3. For the alongshore components, note from Figs. 3 and 4 or from Table 3 that both D_1 and D_2 have negative mean values, the former signifying a southward flowing mean barotropic current

[2] The nominal distance of DB-7 or Carnation from the shore is about 13 km. However, due to the gradual decrease of the water depth as the coastline is approached, it is not clear what the "effective" distance of these stations from the shore is in a constant-depth model like the present. The distance of 10 km is a rough guess.

and the latter a mean shear such that the surface layers flow southward and the bottom layers flow northward. Note that D_1 and D_2 are uncorrelated in time for the alongshore component. However, they are fairly well correlated for the east-west component, especially from 18 July to 1 August (Fig. 5). Note also from Table 3 that the ratios of the standard deviations of the alongshore barotropic and the first baroclinic modal amplitudes are 1.7 for Carnation and 1.9 for DB-7, which is in qualitative agreement with the conclusion of Smith (1974).

It is useful to get an estimate of the residual left after fitting the first two modes to the data series. For this, the alongshore component relative residual at at each point (z,t) is given by

$$\epsilon(z_j, t_k) = \left[\frac{[v(z_j, t_k) - D_1(t_k) - D_2(t_k)Z_2(z_j)]^2}{\frac{1}{K} \sum_{k=1}^{K} v^2(z_j, t_k)} \right]^{\frac{1}{2}},$$

where K is the number of time samples. The overall residual, defined as the time and depth average of $\epsilon(z_j, t_k)$, is 15% for Carnation and 16% for DB-7. A similar calculation was made for the u components, and the residuals were found to be somewhat larger (Table 3).

The baroclinic part of the north-south current at each depth was determined by subtracting the barotropic part $D_1(t)$ from the data $v(z,t)$. The resulting time series for DB-7, which contain not only the first baroclinic mode but also the residual, are shown in Fig. 8. The series for Carnation are similar and are not shown. The time series for 20 m is seen to be almost always out of phase with those for 40, 60 and 80 m, which is consistent with the presence of a first baroclinic mode since the zero crossing of this mode is at about 29 m for Carnation and 27 m for DB-7.

6. Empirical orthogonal decomposition

The dynamic modes computed in the previous section are orthogonal in the continuous sense, but due to the sampling at a finite number of predetermined depths it turns out that the modes are not "discretely orthog-

TABLE 3. Means, standard deviations and correlations of dynamic modes.

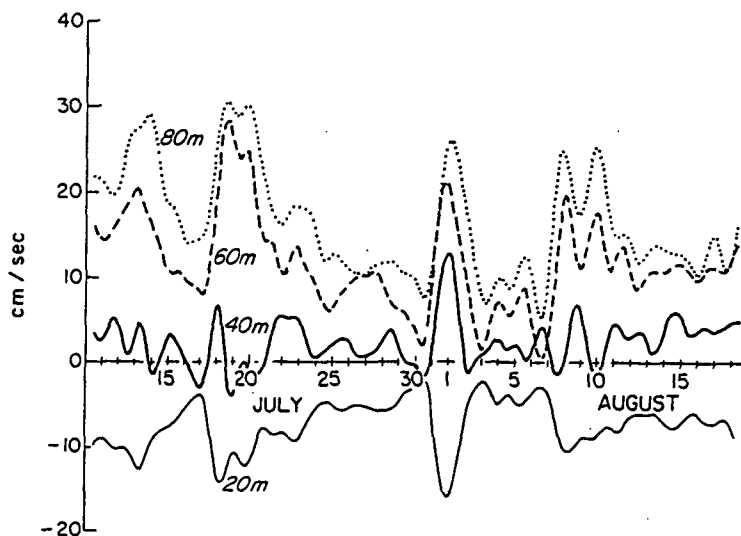|		Carnation		DB-7	
		u	v	u	v
D_1	Mean (cm s⁻¹)	3.1	−15.1	0.8	−10.1
	S.D. (cm s⁻¹)	3.2	9.9	4.7	12.6
D_2	Mean (cm s⁻¹)	1.0	−20.7	−4.6	−17.0
	S.D. (cm s⁻¹)	3.3	5.8	3.4	6.7
Correlation D_1, D_2		0.7	−0.1	0.4	−0.1 .
Relative residual		32%	15%	21%	16%

FIG. 8. The baroclinic component of north–south current at DB-7.

onal" [see Eq. (5.8)]. Moreover, the dynamic modes are dependent on the equations of motion and the boundary conditions used, which are based on several approximations including a flat bottom, linear and inviscid dynamics, etc. The resulting modes can be physically significant only if these approximations are justified.

It is of interest to perform a modal analysis which does not need these series of assumptions. That is, one is interested in modes which are discretely orthogonal, and which do not depend on any dynamic assumptions but only on the statistics of the data. These are provided by the so-called "empirical orthogonal functions." This method was first introduced by Kosambi (1943); excellent discussions of it can be found, for example, in Lumley (1970) and Busch and Petersen (1971). A brief outline of the expansion technique is given below; more details and a short discussion are given in Appendix B.

Let $v_k(z_i)$ denote the value of a variable (in the present case the north–south velocity) at time t_k ($k=1, \ldots, K$) and depth z_i ($i=1, \ldots, N$). Let

$$R(z_i,z_j) = \frac{1}{K} \sum_{k=1}^{K} v_k(z_i)v_k(z_j) \qquad (6.1)$$

denote the matrix of correlation coefficients. Then the eigenvectors $\phi_n(z_j)$ of this real and symmetric matrix, defined by

$$\sum_{i=1}^{N} R(z_i,z_j)\phi_n(z_i) = \lambda_n\phi_n(z_j), \quad n=1, \cdots, N, \quad (6.2)$$

are called the empirical orthogonal eigenfunctions; they obey the orthogonality condition

$$\sum_{i=1}^{N} \phi_n(z_i)\phi_m(z_i) = \delta_{nm}. \qquad (6.3)$$

It is shown in Appendix B that the eigenvalues λ_n are the time average energy in the various modes, and that the sum of the eigenvalues add up to the total energy. Since the set $\{\phi_n\}$ is complete, the time series can be expanded in terms of them, i.e.,

$$v_k(z_i) = \sum_{n=1}^{N} E_{kn}\phi_n(z_i), \qquad (6.4)$$

where the expansion coefficients are given by

$$E_{kn} = \sum_{i=1}^{N} v_k(z_i)\phi_n(z_i). \qquad (6.5)$$

TABLE 4. Empirical eigenfunctions for north–south component (v).

		Mode 1		Mode 2		Mode 3		Mode 4	
		Carnation	DB-7	Carnation	DB-7	Carnation	DB-7	Carnation	DB-7
Eigenvalue λ_n (cm^2 s^{-2})		420.2	684.8	30.0	51.1	8.2	6.6	3.2	2.4
Explained variance $\lambda_n/\Sigma\lambda_n$		91.1%	92.0%	6.4%	6.9%	1.8%	0.9%	0.7%	0.3%
Eigenfunction ϕ_n (z_i)	20 m	0.43	0.43	0.81	0.67	0.39	0.61	0.07	−0.02
	40 m	0.50	0.51	0.14	0.37	−0.85	−0.76	0.60	0.16
	60 m	0.56	0.54	−0.34	−0.39	0.22	0.02	−0.72	−0.75
	80 m	0.50	0.51	−0.45	−0.52	0.27	0.23	0.69	0.64

The north–south components of velocity at Carnation and DB-7 were decomposed into these modes. Although the 95 m current series at Carnation could now have been included since there is no longer any assumption on inviscid dynamics, it was left out so as to be able to compare Carnation results with DB-7 results, and dynamic modes with empirical modes.

Since the behavior of the time variations of the currents are of most interest here, the eigenfunctions were computed after removing the time mean from each record. The computed eigenvalues and eigenfunctions for the longshore component are shown in Table 4. The following points may be noted there:

1) If one imagines that the discrete values defining the eigenfunctions are joined by continuous lines, then the resulting first mode, which is fairly depth-independent, would have no zero crossing, the second one would have one zero crossing, and so on. This sequence, however, is solely a characteristic of the data, and was determined by the ordering of the explained variance. Also, as is explained in Appendix B, the empirical eigenfunctions resemble the dynamic modes if the amplitudes of the latter happen to be uncorrelated in time. The correlation coefficient between the amplitudes D_1 and D_2 for the longshore component did turn out to be very low (~ 0.1), which explains why the empirical modes resemble the dynamic modes for the alongshore component.

2) About 98% of the variance is accounted for by the first two eigenfunctions, with the first one accounting for more than 91%.

3) The first mode, which accounts for most of the energy, is fairly barotropic. Its depth structure signifies that the fluctuations at 60 m are on the average the largest, those at 20 m are the lowest, and those at 40 m and 80 m fall midway between the two, and all these fluctuations are simultaneous and of the same sign. Since this mode accounts for most of the energy, this structure is expected to resemble the pattern of the variation of the rms values (actually, their squares) of the current fluctuations with depth. This is the case, as may be checked from Table 1.

The first two expansion coefficients $E_1(t_k)$ and $E_2(t_k)$, determined by (6.5), are plotted in Fig. 9. For both Carnation and DB-7, the behavior of E_1 and E_2 with time is very similar to the behavior of D_1 and D_2 shown in Figs. 3 and 5, as is expected because of the similarity of the dynamic and empirical mode shapes. It may be mentioned that although the structure of $Z_1(z_i)$ and $\phi_1(z_i)$, $Z_2(z_i)$ and $\phi_2(z_i)$, are only qualitatively similar, their amplitudes $D_1(t)$ and $E_1(t)$, $D_2(t)$ and $E_2(t)$ are very similar; in fact, the correlation coefficient between $D_1(t)$ and $E_1(t)$ is found to be 0.98 for both Carnation and DB-7, and that between $D_2(t)$ and $E_2(t)$ is 0.97 for Carnation and 0.93 for DB-7. Note that the reason
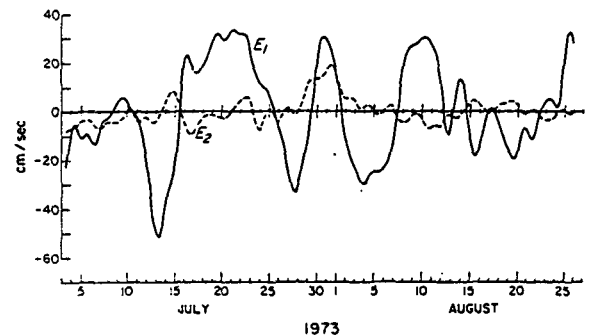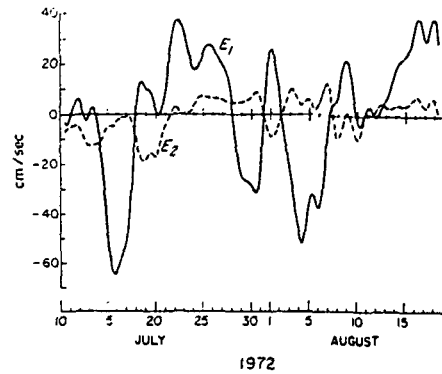

FIG. 9. The amplitudes of the first two empirical modes for the north–south components: top curves for DB-7 and bottom curves for Carnation.

the amplitude of E_1 is larger than that for D_1 is because of different methods of normalization [see (5.6) and (6.3)]. This difference introduces a factor of approximately 2 in the first mode amplitudes, but the second mode amplitudes are comparable. The ratio of the standard deviations of E_1 and E_2 is $(91.4/6.4)^{\frac{1}{2}} = 3.8$ for Carnation, and 3.6 for DB-7. This compares with ratios of S.D. D_1/S.D. $D_2 \sim 1.7$ and 1.9 for Carnation and DB-7, respectively.

The east–west components of the fluctuations were also decomposed into the empirical modes. The results are summarized in Table 5. The larger eigenvalues at DB-7 agree with larger variations of the u component for this station, as shown in Table 1. Also, the empirical modes are much less similar to the dynamic modes for this component, which is a result of the fact that the D_1, D_2 correlation coefficient was not very low for u. The shapes of the first empirical modes are consistent with the pattern of variation of the standard deviation with depth for both stations (Table 1), e.g., maximum at 20 m for Carnation and at 40 m for DB-7. Note that the first empirical eigenfunction for u accounts for about 70% of the variance, compared to about 91% for the v component. Obviously the north–south fluctuations are better correlated in depth.
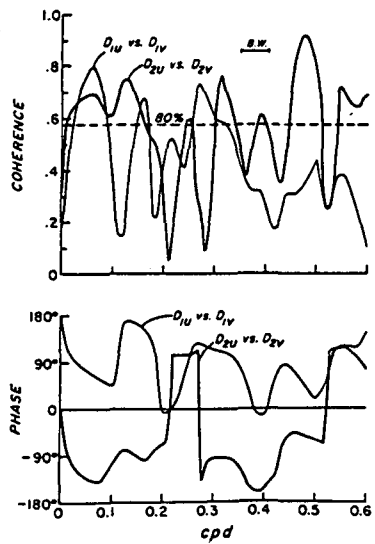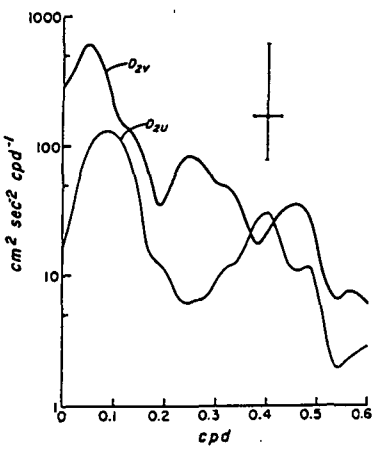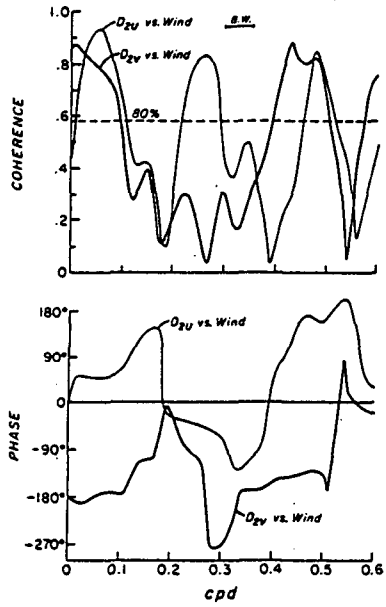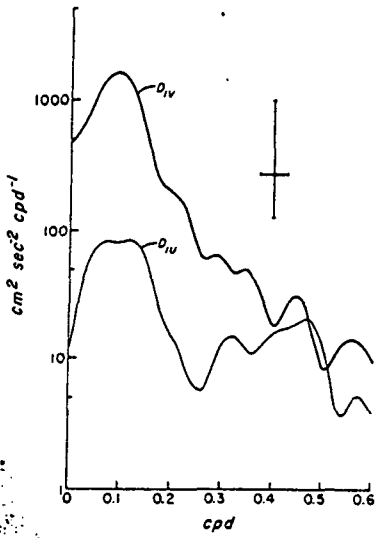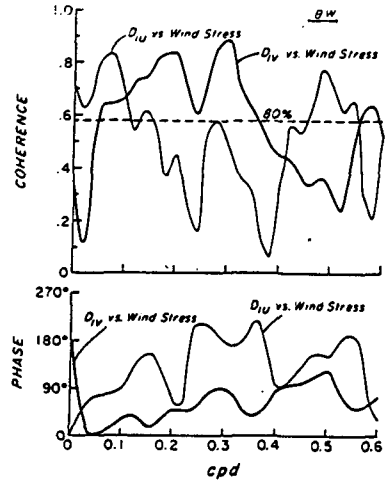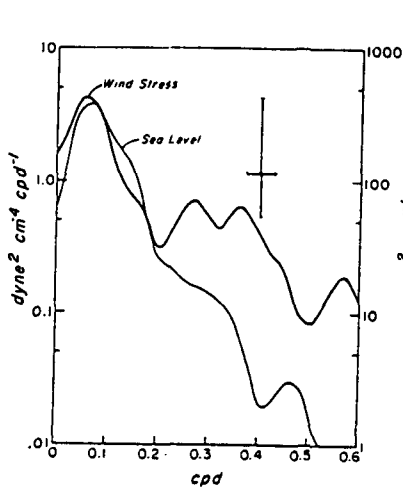
TABLE 5. Empirical eigenfunctions for east–west component (u).

		Mode 1		Mode 2		Mode 3		Mode 4	
		Carnation	DB-7	Carnation	DB-7	Carnation	DB-7	Carnation	DB-7
Eigenvalue λ_n (cm^2 s^{-2})		29.3	79.7	8.9	19.6	2.9	6.9	1.5	1.8
Explained variance $\lambda_n/\Sigma\lambda_n$		68.8%	73.8%	20.1%	18.1%	6.9%	6.4%	3.5%	1.7%
Eigenfunction ϕ_n (z_i)	20 m	0.79	0.52	−0.61	−0.23	0.06	0.81	0.00	0.12
	40 m	0.42	0.63	0.48	−0.52	−0.74	−0.51	−0.20	−0.28
	60 m	0.37	0.48	0.54	0.48	0.66	−0.27	−0.36	0.68
	80 m	0.24	0.32	0.32	0.67	0.10	0.08	0.91	−0.66

7. Relation of the dynamic and empirical modes with the wind stress, sea level and temperature

We examine in this section the relation of the dynamic and the empirical modes with the alongshore component of the wind stress, the sea level, and some of the continuous temperature measurements made at the location of the current meters. The notation D_{nu}, D_{nv}, E_{nu} and E_{nv} will be used to denote the coefficients of the nth modes for u and v. The correlation coefficients between different variables are entered in Table 6.

TABLE 6. Correlation coefficients.

		Carnation	DB-7
Wind stress vs	D_{1v}	0.46	0.63
	D_{2v}	−0.47	−0.42
	E_{1v}	0.54	0.68
	Sea level	0.61	0.62
Sea level vs	D_{1v}	0.74	0.88
	D_{2v}	−0.47	−0.47
	E_{1v}	0.80	0.91
Temperature at 40 m vs	D_{1v}	0.23	0.03
	D_{2v}	−0.07	−0.64
	E_{2v}	0.02	−0.67

These are zero lag values, but, for the coefficients listed, the maximum absolute value of the correlation coefficient occurred either at zero lag or close to it (i.e., within one day). In all cases the correlation was computed by removing the temporal mean, except for those involving the temperature for which the appreciable linear trend due to seasonal heating was removed. The north–south (alongshore) component of the wind stress was computed from the hourly values of the wind stress vector and then low-pass filtered in the same manner as the currents. The formula used was

$\tau_W = \rho_A C_D (u_W^2 + v_W^2)^{\frac{1}{2}} v_W$ [dyn cm^{-2}], where u_W and v_W are the wind velocity components, the air density $\rho_A = 1.23 \times 10^{-3}$ g cm^{-3}, and $C_D = 1.4 \times 10^{-3}$. The time series of τ_W is quite similar in appearance to that for the v component of the wind, shown in Fig. 5, except that the peaks are accentuated in the τ_W plot.

Since some of the spectral quantities for the 1972 DB-7 measurements have already been presented in Smith (1974), and since the record lengths for Carnation are greater, we shall present here the spectral quantities for Carnation only. Autospectra of the north–south component of the wind stress τ_W, sea level, and the dynamic modes D_{1v}, D_{1u}, D_{2v} and D_{2u} for the 1973 measurements are given in the left column of Fig. 10. The coherence and phase between the various pairs are given in the right column of the same figure.

On comparing the 1973 series of D_{1v} with that of the wind (Fig. 3) it may be noted that the wind appears to have a great deal of high-frequency (i.e., periods of 2–3 days) energy that the barotropic component does not have. The spectra (Fig. 10) bear out this point. The wind stress spectrum falls off much less rapidly with increasing frequency than does the spectrum of D_{1v}.

We note from Table 6 that the wind stress and the barotropic mode D_{1v} are positively correlated for both DB-7 and for Carnation. The correlation is not very high, however, and an examination of the time series shows several instances where there are changes in D_{1v} which are not related to the local wind stress. For example, the large changes in the currents at Carnation during the period 28 July–3 August are evidently not related to the local wind variations. That event is presumably due to the propagation or advection of a particular disturbance.

The correlation between the wind stress and D_{2v} (Table 6) is negative. This means that the north–south baroclinic fluctuation in the surface layer is mostly northward when the wind is southward. This result also

FIG. 10. Spectral quantities of the north–south component of the wind stress, sea level, and the barotropic and first baroclinic components of the currents at Carnation. The autospectra are given in the left column, and the coherence and phase spectra given in the right column. The superscript v refers to the north–south component, u to the east–west component. The phase is positive if the second signal is leading the first, e.g., at 0.3 cpd the wind stress leads D_{1v} by about 90°. The bandwidth and the 95% confidence interval are indicated in the autospectra and the 80% significance level is indicated in the coherence spectra.

shows up in the phase spectrum between the two (Fig. 10) and will be commented on in Section 8.

The barotropic mode D_{1v} is highly correlated with sea level for both Carnation and DB-7. The correlation is positive, which implies that southward currents (negative D_{1v}) are accompanied by lowered sea level at the coast and this is, of course, consistent with a barotropic, geostrophically balanced alongshore current. The modal amplitude of the first empirical eigenfunction, E_{1v}, is slightly better correlated than D_{1v} with the wind stress and sea level for both Carnation and DB-7.

A rough estimate for an offshore scale L of the coastal response may be obtained from a comparison of the change in sea level Δh at the coast and the corresponding change ΔD_1 in the barotropic component of v at DB-7. From Fig. 4, we find $\Delta h = 30$ cm, $\Delta D_1 = 50$ cm s^{-1} during 16–22 July 1972. Assuming, for simplicity, an exponential decay of the barotropic component $\Delta v_1(x) = \Delta D_1 \exp[(x-x_0)/L]$, where $x_0 \approx -10$ km corresponds to the location of DB-7, and utilizing the relation

$$\Delta h = (f/g) \int_0^{-\infty} \Delta v_1 dx$$

for a geostrophically balanced v_1 with $h(-\infty)=0$, we obtain an e-folding scale of $L \approx 50$ km, which is in qualitative agreement with that observed (Kundu and Allen, 1975).

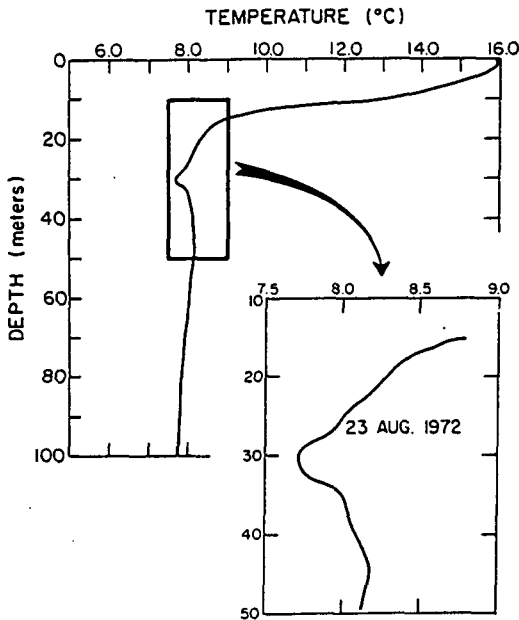It is of interest to check the correlation of the dynamic modes with the temperature measurements. If we assume that the temperature variations will reflect density variations, then we expect the temperature fluctuations to be related to the baroclinic mode. Because of (5.1) and the hydrostatic relation (A2d), the density mode will be given by the z-derivative of the mode shape Z_n. Thus, the first baroclinic density mode has nodes at the top and bottom, and an antinode coinciding with the point of maximum $|Z_{nz}|$. The largest fluctuation in ρ may be expected near this antinode, which appears to be (Fig. 7) somewhat above the zero crossing of $Z_n(z)$. The density in the region of these experiments, however, is strongly controlled by the salinity. In fact, all the density data from which $N(z)$ was calculated for DB-7 showed a temperature inversion at about 40 m (Fig. 11). The temperature at Carnation also showed an inversion near 40 m, but it was much weaker than that at DB-7 and in many cases the temperature was nearly constant with depth near 40 m.

The temperature measurements at 20 m showed relatively large fluctuations which were evidently not related to the baroclinic velocity field but were probably related to events in the mixed layer. The temperature measurements at 60 and 80 m show variations of very small magnitude, and are not very reliable. We concentrate, therefore, on examining the 40 m temperature measurements. A comparison of the time series of the 40 m temperature, $T_{40\,m}$, at DB-7, shows a strong visual correlation with the series for D_{2v} and E_{2v}. Those series are plotted in Fig. 12 where, for the sake of comparison, the linear trend is removed from each series. The similarity is evident. The correlation coefficients (Table 6) are correspondingly relatively high (-0.64 and -0.67). Note that the sign of the correlation is determined by the sign used in defining the eigenfunction Z_2. According to our definition (Fig. 6), the observed sign of the correlation means that a positive temperature fluctuation at 40 m was accompanied by a southward baroclinic velocity fluctuation in the surface layer, as can also be seen by comparing the temperature series in Fig. 12 with the baroclinic longshore velocity series in Fig. 8. This behavior is expected from the thermal wind relation if the baroclinic components are assumed to decay in the offshore direction and only if a temperature inversion, i.e., a negative temperature gradient, exists near 40 m.

It may be mentioned that for Carnation the 40 m temperature was poorly correlated with D_{2v} and E_{2v}, which is possibly due to the fact, mentioned before, that the temperature gradients were extremely weak near 40 m at Carnation.

At DB-7, where $T_{40\,m}$ and D_{2v} were fairly well correlated, a corresponding check of the correlation coefficient of $T_{40\,m}$ with the barotropic mode D_{1v} showed a negligible correlation. Since the vertical movement of density surfaces due to the barotropic mode should be much smaller than their movement due to the baroclinic mode, this gives us some confidence in the modal decomposition and in the representation of baroclinic
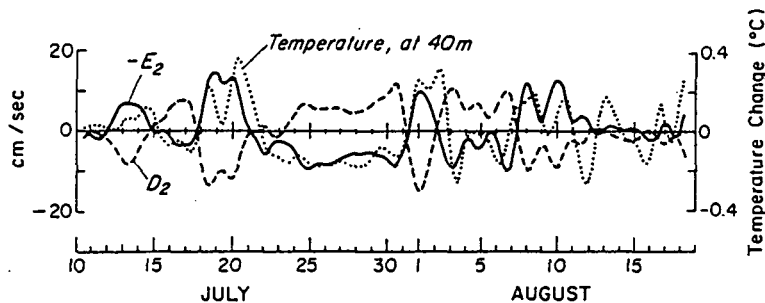

Fig. 11. A typical vertical temperature profile near DB-7 taken on 23 August 1972 [cast number 480 of Halpern and Holbrook (1972)].

FIG. 12. Comparison of the temperature at 40 m with the amplitudes of the second dynamic and empirical eigenfunctions for the north–south components. The E_2 series is plotted with its sign changed for clearer visibility. The linear trend is removed from all series, although it was appreciable only for the temperature series.

velocities by D_{2v}. Continuous measurements of both salinity and temperature, so that a time series for density could be calculated, would, of course, provide a means for a better check.

Referring to the autospectra plotted in Fig. 10, we note that the most conspicuous general feature is a low-frequency peak in all spectra at frequencies between 0.06 and 0.1 cpd. The peak in the wind stress τ_W and in D_{2v} is around 0.06 cpd while that for D_{1v} is higher, near 0.09 cpd, and that for sea level is somewhere between these two.

Near the frequency 0.06 cpd where the autospectrum of the wind stress τ_W has a peak, the values of the coherence between D_{1u} and τ_W, denoted by D_{1u} vs τ_W, and that between D_{2u} vs τ_W are relatively high. The coherence D_{1v} vs τ_W and D_{2v} vs τ_W are also relatively high near this frequency and likewise so are the coherence D_{1u} vs D_{1v} and D_{2u} vs D_{2v}.

The values of the phase spectra in these regions of high coherence are also of interest. We shall discuss in Section 8 some consequences, with respect to phase, of simple theoretical models of wind-stress-forced barotropic and baroclinic motion on the continental shelf and slope and attempt to relate them to the present measurements. For convenience, we have listed in Table 8 the values of the coherence and phase for the various components mentioned above.

There are several other peaks in the autospectra and coherence spectra at higher frequencies. We point out two frequencies, one in connection with the barotropic mode and the other in connection with the baroclinic mode, where there is simultaneously a high coherence between the wind stress and both the u and the v components and also a high coherence between the u and v components themselves. These are seen in Table 7.

Although the spectral calculations for 1972 from DB-7 have not been presented, we mention one point from those results in connection with the low-frequency $\omega = 0.06$ cpd behavior found in the 1973 Carnation records. A very similar low-frequency behavior is evident in the 1972 results. There is a large peak in the autospectrum of the alongshore component of the wind

stress, in that case near $\omega = 0.14$ cpd, which is accompanied by large relative values of the coherence between D_{1v} vs τ_W, D_{1u} vs τ_W and D_{1u} vs D_{1v}. There is also a peak in the autospectrum of D_{1u} near that frequency and high values, although not a peak, in the autospectrum of D_{1v}. The values of the phase between the variables mentioned above are similar to those from 1973 near 0.06 cpd and are listed, with the values of the coherence, in Table 7. These features are also evident in the presentation of the 1972 results by Smith (1974).

8. Dynamical discussion

An idealized model for the motion of coastal waters in response to meteorological forcing is discussed in Appendix A. One very useful result from that model

TABLE 7. Values of the coherence and phase at selected frequencies. For the phase, the second variable leads if the value is positive.

Frequency		Coherence	Phase
	1973		
0.06 cpd	D_{1v} vs τ_W	0.65	$10° \pm 38°$
	D_{1u} vs τ_W	0.83	$80° \pm 23°$
	D_{1u} vs D_{1v}	0.80	$70° \pm 32°$
	D_{2v} vs τ_W	0.78	$-180° \pm 27°$
	D_{2u} vs τ_W	0.94	$45° \pm 7°$
	D_{2u} vs D_{2v}	0.68	$-135° \pm 35°$
0.28 cpd	D_{1v} vs τ_W	0.90	$90° \pm 15°$
	D_{1u} vs τ_W	0.60	$200° \pm 45°$
	D_{1u} vs D_{1v}	0.74	$120° \pm 30°$
0.48 cpd	D_{2v} vs τ_W	0.94	$-130° \pm 7°$
	D_{2u} vs τ_W	0.84	$170° \pm 23°$
	D_{2u} vs D_{2v}	0.94	$-60° \pm 7°$
	1972		
0.14 cpd	D_{1v} vs τ_W	0.96	$19° \pm 7°$
	D_{1u} vs τ_W	0.82	$83° \pm 32°$
	D_{1u} vs D_{1v}	0.90	$62° \pm 18°$

is the fact that the time-dependent alongshore behavior of both the barotropic and baroclinic components of the motion is governed by a forced, first-order wave equation, where the alongshore component of the wind stress τ_W is the forcing mechanism (Gill and Schumann, 1974; Gill and Clarke, 1974). Some examples of the solutions to this equation, with simple representations for τ_W, are given in Appendix A. We discuss below some results from these examples in relation to the values of the phase spectra at frequencies where the coherence between the wind stress and the dynamic modes is relatively high. These frequencies were pointed out in Section 7 and the quantities of interest are summarized in Table 7.

Some of the conclusions we draw here, based on measurements at a single station, certainly have to be regarded as tentative. This is especially true when they concern results which follow from an alongshore propagation or an alongshore distribution of the wind stress, with a consequent response of the currents that varies in the alongshore direction. We feel, nevertheless, that it is worthwhile to examine the present single-station records in light of the simple results from Appendix A.

We first consider the barotropic components and refer to the results in Table 7 for the frequencies $\omega = 0.06$ cpd for 1973 and $\omega = 0.14$ cpd for 1972. The frequency, $\omega = 0.06$ cpd, is characterized by a peak in the auto-spectrum of the wind stress and, relative to higher frequencies, a great deal of energy in the barotropic component D_{1v}. With regard to the phases, one important point is the very small lag ($\sim 10°$) of D_{1v} with the wind stress τ_W. In addition to the small phase lag of D_{1v} with τ_W, the phase results also show that τ_W leads D_{1u} by about $80°$ and that D_{1v} leads D_{1u} by approximately $70°$. Similar behavior was found in the 1972 measurements at $\omega = 0.14$ cpd. There is a peak in the autospectrum of the wind stress τ_W and a small phase lag of D_{1v} with τ_W ($\sim 19°$). In addition, τ_W leads D_{1u} by about $83°$ and D_{1v} leads D_{1u} by approximately $62°$.

TABLE 8. Summary of the time phase relation of $v_{(1)}$, $u_{(1)}$ and u_3 with the wind stress τ_W. The phase is the value by which the second quantity leads, if it is positive, or lags, if it is negative.

τ_W	$v_{(1)}$ vs τ_W	Phase $u_{(1)}$ vs τ_W	u_3 vs τ_W
Independent of y: (A33) [or (A35) with $l=0$].	90°	—	180°
Traveling wave (A35) ($\omega \gtrless 0$).			
$(a_1^{-1}\omega + l) > 0$	90°	0°, 180°**	180°
$(a_1^{-1}\omega + l) < 0$	−90°	0°	180°
$(a_1^{-1}\omega + l) = 0$ (resonance)	0°	90°	180°
Standing wave (A45) ($\omega \gtrless 0; l \gtrless 0$).			
$a_1^{-1}\omega \gg l$	90°	−90°, 90°**	180°
$a_1^{-1}\omega \ll l$	0°, 180°**	0°	180°
$a_1^{-1}\omega = l$ (resonance)	0°	90°	180°

* The phase is 0° for $l > 0$ and is 180° for $-a_1^{-1}\omega < l < 0$.
** The phase may be either of these two values depending on the value of

In reference to the results presented in Appendix A and summarized in Table 8, we can make the following points. The small phase lag of D_{1v} with the wind stress and the approximate 90° lag of D_{1u} with τ_W is definitely not consistent with a local two-dimensional, i.e., y-independent, driving of the currents by the wind stress. In that case, D_{1v} should lag τ_W by 90° and D_{1u} should be 180° out of phase with τ_W. In fact, the closest agreement of the observed barotropic phase results at 0.06 cpd for 1973 and at 0.14 cpd for 1972 with the theoretical examples in Table 8 is with the case where the wind stress is represented by a traveling wave and where there is a resonant response. In this model, resonance results if an alongshore component of the wind stress τ_W travels northward along the coast as a wave with the same alongshore wavelength and phase speed as a free, long (i.e., nondispersive) continental shelf wave. Solutions from the theoretical model (Appendix A) indicate that, in the resonant case, the time variation of D_{1v} may be in phase with τ_W and D_{1u} may lag τ_W and D_{1v} by 90°. These results are similar to those in Table 8 for the barotropic components at 0.06 cpd (1973) and at 0.14 cpd (1972).

For the Oregon coast, typical values of phase speeds for the first and second mode barotropic shelf waves, in the long wave limit, are $a_1 \approx 400$ km day^{-1} and $a_2 \approx 100$ km day^{-1} (Cutchin and Smith, 1973). At a frequency of $\omega \approx 0.06$ cpd this implies an alongshore wavelength, for resonance, of $\delta_{y1} \approx 6670$ km for the first mode and $\delta_{y2} \approx 1670$ km for the second. For the corresponding 1972 frequency of $\omega \approx 0.14$ cpd, we obtain $\delta_{y1} \approx 2860$ km and $\delta_{y2} \approx 710$ km.

It is conceivable, based on these results, that a considerable amount of the low-frequency energy in the barotropic component of the currents on the continental shelf is transferred from the atmosphere to the ocean by a resonant, or near-resonant, condition between the alongshore component of the wind stress and long, barotropic continental shelf waves. The idea of a resonant response of forced shelf waves was originally given by Robinson (1964) and was later expanded on in more detail by Mysak (1967). This picture is at least consistent with the phase relationships, which were similar in the measurements from both years, of the barotropic components of the currents D_{1v} and D_{1u} with the wind stress τ_W. It is also consistent with the result that the autospectrum of D_{1v} falls off with increasing frequency much more rapidly than the autospectrum of the wind stress τ_W. It appears, from that fact, that the energy of the wind at low frequency is more efficiently transmitted to the barotropic component of the alongshore current than the energy at higher frequencies. A resonant condition may well provide the mechanism for an efficient energy transfer.

For the barotropic component in 1973 at the higher frequency, $\omega = 0.28$ cpd, we see from Table 7 that D_{1v} lags τ_W by about 90°, D_{1u} lags τ_W by about 200° and

D_{1u} lags D_{1v} by approximately 120°. In contrast to the lower frequency, these results are in fact reasonably consistent with a local, y-independent driving of the currents by the wind stress, as shown in Table 8. Why this type of driving might appear at such a frequency is not clear, but we do note that there is a definite peak in the wind stress autospectrum near 0.28 cpd.

In connection with the baroclinic component, if the ocean responds to τ_W as predicted in the idealized theoretical model in Appendix A, then we would expect the directly forced parts of D_{1v} and D_{2v}, since their alongshore and time-dependent behavior is governed by similar equations (Appendix A), to be coherent with τ_W at the same frequencies. We find, however, that D_{1v} and D_{2v} have a negligible correlation at zero lag (Table 3) and that, in general, the coherence spectra of D_{1v} and D_{2v} vs τ_W (Fig. 10) differ considerably. In addition to this point, direct explanations for the behavior of the baroclinic components at the frequencies $\omega = 0.06$ cpd and $\omega = 0.48$ cpd in Table 7, are not readily found. It is pointed out in Appendix A that, according to the present model, D_{2u} should be 180° out of phase with τ_W. This is close to what is found at the higher frequency, $\omega = 0.48$ cpd, but at the lower frequency $\omega = 0.06$ we find that D_{2u} lags τ_W by 45°.

The most puzzling behavior, however, is found with the v component. At $\omega = 0.06$ cpd, D_{2v} is approximately 180° out of phase with τ_W, whereas at $\omega = 0.48$ cpd, τ_W lags D_{2v} by 130°. This phase behavior of D_{2v} vs τ_W is also reflected in the negative correlation coefficient of D_{2v} and τ_W at zero lag (Table 6) which is found at both Carnation and DB-7. Of the examples presented in Table 8, the only case where D_{2v} could be 180° out of phase with τ_W is the one where the wind stress is in the form of a standing wave and where $c_2^{-1}\omega \ll l$, so that the balance in the y momentum equation is approximately geostrophic. In terms of ω (in cpd) and an alongshore wavelength of δ_y(km), the latter condition is

$$\omega \delta_y c_2^{-1} \ll 1. \qquad (8.1)$$

With $c_2 \approx 50$ km day^{-1} (Appendix A), Eq. (8.1) is satisfied for $\omega = 0.06$ and $\omega = 0.48$ if $\delta_y \ll 800$ km and $\delta_y \ll 104$ km, respectively.

It seems possible that, compared with the barotropic mode, the baroclinic mode may effectively see the wind stress on shorter alongshore scales. This could be because the baroclinic mode exists in a narrow region, of onshore–offshore scale of the order of 10–15 km, for which alongshore coastline and bottom topographic variations could have a relatively larger effect in causing alongshore variations in the motion than they have for the barotropic mode, which has a greater onshore–offshore scale. Also, the density structure within the 10–15 km wide region, and, therefore the basic state upon which the response depends, may actually vary considerably in the alongshore direction.

If the baroclinic mode is capable of responding on relatively short alongshore scales, then the satisfaction of a condition like (8.1) may be reasonable.

It is not clear, however, how to reconcile, at the low frequency $\omega = 0.06$ cpd, the standing wave distribution of the stress, which may provide a possible rationalization of the behavior of the D_{2v} component, with the traveling wave wind stress distribution which was used in an attempt to explain the barotropic behavior. In addition, at the higher frequency $\omega = 0.48$, the satisfaction of (8.1) requires alongshore wavelengths that seem rather small, i.e., $\delta_y \ll 100$ km. We conclude, therefore, that at this point the behavior of the baroclinic component remains somewhat of a puzzle. Hopefully, a more complete picture of the baroclinic behavior will emerge when the full set of current meter measurements from CUE-I and CUE-II are analyzed and are decomposed into barotropic and baroclinic modes.

9. Summary

Low-frequency ($\omega < 0.6$ cpd) variations in the currents in 100 m of water on the continental shelf off the coast of Oregon during two upwelling seasons have been investigated. The currents were measured at two stations. One station, DB-7, was maintained for 48 days during the summer of 1972 as part of CUE-I and the other station, Carnation, was maintained for 54 days during the summer of 1973 as part of CUE-II. The current measurements were made at 20, 40, 60 and 80 m depths at DB-7 and at 20, 40, 60, 80 and 95 m depths at Carnation. The north–south (approximately alongshore) v and the east–west (approximately onshore–offshore) u components of the currents have been decomposed into two types of modal structure in the vertical direction. The two modal structures are 1) the dynamic modes, provided by the separable solution of idealized governing equations and boundary conditions and 2) empirical orthogonal modes, which depend only on the statistics of the data. For the dynamic modes, the barotropic (depth-independent) and the first baroclinic mode have been fitted to the measurements by minimizing the squared residual. The time-dependent behavior of the modal coefficients has been compared with the time variations in the wind, the sea level, and the continuous temperature measurements made at the location of the current meters.

Qualitatively, the results from the two separate upwelling seasons are quite similar. When the results are summarized below without reference to the year it implies that the conclusion holds for both years.

The dynamic barotropic mode for the alongshore component of the current, D_{1v}, has a negative mean value, which implies a mean southward barotropic flow. The first baroclinic dynamic mode, D_{2v}, also has a negative mean value, which implies a mean shear in the current such that there is a southward flow near the

surface and a northward flow near the bottom. The standard deviation of the barotropic component D_{1v} is found to be twice as large as that of the baroclinic component D_{2v}. The major fluctuations of the alongshore component of the currents are therefore barotropic. It is also found that the barotropic mode D_{1v} is very well correlated with sea level and that, at DB-7, the baroclinic mode D_{2v} is correlated with the temperature fluctuations at 40 m.

The first empirical eigenmode of the alongshore component of velocities, E_{1v}, accounts for about 91% of the energy and is fairly depth-independent in structure. It is also extremely well correlated with the barotropic dynamic mode D_{1v} and is slightly better correlated with sea level than D_{1v} is. The second empirical eigenmode E_{2v} accounts for about 7% of the energy and resembles the first baroclinic dynamic mode in vertical structure.

Calculations for the 1973 measurements of the autospectra of the north–south component of the wind stress τ_W, the sea level, and the dynamic modes D_{1v}, D_{1u}, D_{2v} and D_{2u} show a low-frequency peak in all spectra between 0.06 and 0.1 cpd. Near the frequency 0.06 cpd, the values of the coherence between the dynamic modes and the wind stress τ_W and between the respective u and v components of the dynamic modes, i.e., between D_{1u} vs D_{1v} and D_{2v} vs D_{2u}, are relatively high. The low-frequency behavior of the barotropic mode at 0.06 cpd is characterized by a small ($\sim 10°$) phase lag of D_{1v} with τ_W and an approximate 80° phase lag of D_{1u} with τ_W. In the 1972 measurements, there is a similar low-frequency behavior near $\omega = 0.14$ cpd, i.e., there is a peak in the autospectrum of the wind stress and high values of the coherence between D_{1u} vs τ_W, D_{1v} vs τ_W, and D_{1u} vs D_{1v}. The phase lag of D_{1v} with τ_W is small ($\sim 19°$) and the phase lag of D_{1u} with τ_W is about 80°, similar to the phase results from 1973 at 0.06 cpd. In the 1973 results there are also relatively high values of the coherence for the barotropic mode between the currents and the wind stress and between the u and v components of the currents, i.e., between D_{1u} vs τ_W, D_{1v} vs τ_W, and D_{1u} vs D_{1v} at the higher frequency of 0.28 cpd.

An idealized theoretical model for wind-driven motion on a continental shelf and slope was utilized to provide information on the phase relationships of the wind stress with the barotropic and baroclinic u and v components of the currents. The phase values for D_{1v} vs τ_W and D_{1u} vs τ_W at 0.06 cpd in 1973 and at 0.14 cpd in 1972 are consistent with the theoretical results for the resonant response of long, barotropic continental shelf waves to an alongshore component of the wind stress traveling northward along the coast as a wave. The observed phase values of the barotropic components at the higher frequency 0.28 cpd are, in contrast, reasonably consistent with a local, i.e., alongshore, independent driving of the barotropic currents by a time-varying wind stress.

APPENDIX A

Theoretical Considerations

We utilize the following conceptual picture for the response of the ocean in this coastal region to meteorological forcing (Allen, 1975a). We expect a baroclinic response, involving forced internal Kelvin waves, in a narrow region over the continental shelf and near the coast with an onshore-offshore scale the order of the internal Rossby radius of deformation $\delta_R = HN/f$, where H is a characteristic depth, N a characteristic Brunt-Väisälä frequency, and f the Coriolis parameter. For typical values of $H = 100$ m, $N = 2^{\frac{1}{2}} \times 10^{-2}$ s^{-1} (corresponding to a $\Delta\rho/\rho_0 = 2 \times 10^{-3}$ over H) and $f = 10^{-4}$ s^{-1}, we find $\delta_R \approx 14$ km. We also expect a barotropic response, consisting of forced continental shelf waves, which extends over a broader region with offshore scale the order of the width L of the continental shelf and slope. Off the Oregon coast, $L \approx 120$ km.

It was shown by Allen (1975a) for a two-layer coastal model that the barotropic and baroclinic components of the motion would be coupled if the parameter $\lambda = \delta_R/\delta_B$ is $O(1)$, where δ_B is a characteristic scale length of the bottom topography, given by $\delta_B = |H/H_x|$.[3] It was also shown that, on the Oregon continental shelf (i.e., for $|x| < 30$ km) during the upwelling season, λ has values that are close to $O(1)$. The determination of the coupled modes of motion when $\lambda = O(1)$, however, appears to be a difficult problem. In order to make some progress in decomposing the velocity field into barotropic and baroclinic components we will proceed and assume that $\lambda \ll 1$, in which case the baroclinic and barotropic components are uncoupled, and hope that the most essential dynamics are retained. As a result, the forced baroclinic response, within δ_R of the coast, effectively feels only a flat bottom in the first approximation (Allen, 1975a). We complete the model by adding a vertical wall to represent the coastal boundary.

---

[3] The coordinate system is defined in the main text (Section 4). Here we assume that the coastline is straight and is aligned with the y axis and that the origin is placed at the coast and on the bottom.

We first formulate the baroclinic problem. Consider an incompressible fluid which satisfies the Boussinesq approximation and which is situated on an f plane which effectively rotates with uniform angular velocity $\Omega = \frac{1}{2}f\hat{k}$. The problem is linearized by the assumption that the motion results in negligible nonlinear fluid accelerations and in small departures from an equilibrium, stable density distribution $\bar{\rho}(z)$. The hydrostatic approximation is utilized. We consider inviscid motion away from frictional regions, i.e., away from the surface layer, the bottom boundary layer and the very nearshore region. We will assume in addition that the typical alongshore y scales, δ_y, are considerably larger than x scales, δ_x, and that the time scale δ_t is greater than f^{-1}, i.e., that

$$\delta_y \gg \delta_x, \quad f\delta_t \gg 1. \tag{A1a, b}$$

The resulting equations are

$$u_x + v_y + w_z = 0, \tag{A2a}$$

$$-fv = -p_x/\rho_0, \tag{A2b}$$

$$v_t + fu = -p_y/\rho_0, \tag{A2c}$$

$$0 = -p_z - \rho g, \tag{A2d}$$

$$\rho_t + w\bar{\rho}_z = 0, \tag{A2e}$$

where (u,v,w) are the velocity components in the (x,y,z) directions, ρ is the perturbation density field, ρ_0 a reference density, and g the acceleration of gravity. The geostrophic balance in (A2b) follows from (A1).

It is assumed that the motion is driven by an alongshore component of the wind stress τ_W which does not vary appreciably with x over the shelf-slope width scale L ($L \gg \delta_R$). The wind stress acts as a driving mechanism through the suction of fluid into the surface layer at the coast ($x=0$, $z=H$) (Allen, 1973). The surface is assumed to be a rigid lid and the boundary conditions at $z=0$, H are

$$w = 0, \quad z = 0, H. \tag{A3}$$

Eqs. (A2) may be combined into an expression for the conservation of potential vorticity which may be written in terms of the pressure alone and integrated with respect to time. Assuming that the initial potential vorticity is equal to zero, we obtain

$$p_{xx} + (f^2 N^{-2} p_z)_z = 0, \tag{A4}$$

where $N^2 = -g\bar{\rho}_z/\rho_0$ is the square of the Brunt-Väisälä frequency. In terms of p, (A3) becomes

$$p_z = 0, \quad z = 0, H. \tag{A5}$$

Eq. (A4) with boundary condition (A5) may be solved by a separation of variables,

$$p = \sum_{n=1}^{\infty} Y_n(y,t) X_n(x) Z_n(z), \tag{A6}$$

where, from (A4),

$$X_{nxx} - \gamma_n^2 X_n = 0, \tag{A7}$$

$$(S^{-1} Z_{nz})_z + \gamma_n^2 Z_n = 0, \tag{A8}$$

where $S = N^2/f^2$, γ_n is the separation constant, and where (A5) requires

$$Z_{nz} = 0, \quad z = 0, H. \tag{A9a, b}$$

The appropriate solution to (A7) is $X_n = \exp(\gamma_n x)$. Eq. (A8) with boundary conditions (A9) defines an eigenvalue problem for γ_n. Similar separable solutions for coastal problems were obtained by Walin (1972) and by Gill and Clarke (1974) [see also Mooers and Allen (1973)].

If the motion is forced by an alongshore component of the wind stress $\tau_W(y,t)$, then the boundary condition at $x=0$ may be written as (Pedlosky, 1974; Mooers and Allen, 1973)

$$\rho_0 fu = -(p_y + f^{-1} p_{zt}) = -\tau_W \delta(z-H), \quad x = 0, \tag{A10}$$

where $\delta(z-H)$ is the Dirac delta function. Eq. (A10) represents the suction into the surface Ekman layer at the coast.

An equation for Y_n results from the application of (A10) and is

$$c_n^{-1} Y_{nt} + Y_{ny} = \tau_{Wn}(y,t), \quad n = 2, 3, \ldots, \tag{A11}$$

where $c_n = f\gamma_n^{-1}$ and where τ_{Wn} is defined by the expansion

$$\tau_W(y,t)\delta(z-H) = \frac{1}{2}\tau_W H^{-1} + \sum_{n=2}^{\infty} \tau_{Wn} Z_n. \tag{A12}$$

[The $n=1$ solutions are taken to be $Z_1 =$ constant, $X_1 =$ constant, and they correspond to the representation, within $|x| \lesssim O(\delta_R)$, of the barotropic solution, which varies on the larger scale $\delta_x = L \gg \delta_R$.] We see that Y_n satisfies a forced first-order wave equation (Gill and Clarke, 1974). Note that c_n is the phase velocity for free internal Kelvin waves. Using γ_n from Table 3, we find, e.g., for Carnation, that $c_2 = 54$ cm s^{-1} and $c_3 = 26.5$ cm s^{-1}.

Since a mean baroclinic alongshore current, with accompanying onshore–offshore density gradients, exists on the shelf during the upwelling season (Smith, 1974; see also Table 1), we should assess the validity of the assumption of negligible nonlinear advective effects. To do this, we now formulate the problem with a mean alongshore current.

Let us denote the total velocity compoents by $(\tilde{u}, \tilde{v}, \tilde{w})$ and the full pressure and density by $\tilde{p}$ and $\tilde{\rho}$. We assume that

$$\tilde{v} = \bar{v}(x,z) + v + \cdots, \tag{A13a}$$

$$\tilde{u} = u + \cdots, \tag{A13b}$$

$$\tilde{w} = w + \cdots, \tag{A13c}$$

$$\tilde{\rho} = \bar{\rho}(x,z) + \rho + \cdots, \tag{A13d}$$

$$\tilde{p} = \bar{p}(x,z) + p + \cdots, \tag{A13e}$$

where the variables in the basic state satisfy

$$f\bar{v}=\frac{\bar{p}_x}{\rho_0}, \quad \bar{p}_z=-g\bar{\rho}, \quad \bar{v}_z=-\frac{g}{f}\frac{\bar{p}_x}{\rho_0}. \quad \text{(A14a, b, c)}$$

The resulting equations for the perturbations are

$$u_x+v_y+w_z=0, \quad \text{(A15a)}$$

$$(u_t+\bar{v}u_y)-fv=-p_x/\rho_0 \quad \text{(A15b)}$$

$$v_t+u\bar{v}_x+\bar{v}v_y+w\bar{v}_z+fu=-p_y/\rho_0 \quad \text{(A15c)}$$

$$0=-p_z-\rho g, \quad \text{(A15d)}$$

$$\rho_t-\frac{f\rho_0}{g}\bar{v}_zu+\bar{v}\rho_y-\frac{\rho_0}{g}N^2w=0, \quad \text{(A15e)}$$

where $N^2(x,z)=-g\bar{p}_z/\rho_0$. The terms in the parentheses in (A15b) may be neglected with assumptions (A1). If a potential vorticity equation is formed from (A15), the result is

$$\frac{\partial}{\partial x}\left\{\left(\bar{v}_x+f-\frac{f\bar{v}_z^2}{N^2}\right)^{-1}\left[-p_y-\frac{p_{xt}}{f}-\frac{\bar{v}p_{xy}}{f}+\frac{\bar{v}_z}{N^2}(p_{zt}+\bar{v}p_{yz})\right]\right\}$$

$$+\frac{p_{xy}}{f}+\frac{\partial}{\partial z}\left\{-\frac{1}{N^2}(p_{zt}+\bar{v}p_{yz})-\frac{f\bar{v}_z}{N^2}\left(\bar{v}_x+f-\frac{f\bar{v}_z^2}{N^2}\right)^{-1}\right.$$

$$\left.\times\left[-p_y-\frac{p_{xt}}{f}-\frac{\bar{v}p_{xy}}{f}+\frac{\bar{v}_z}{N^2}(p_{zt}+\bar{v}p_{yz})\right]\right\}=0. \quad \text{(A16)}$$

Eq. (A16) reduces to (A4) if

$$R_1=\frac{U}{\delta_z f}\ll1, \quad R_2=\frac{U^2}{\delta_z^2 N_m^2}\ll1, \quad \text{(A17a, b)}$$

$$R_3=\frac{U\delta_t}{\delta_y}\ll1, \quad R_4=\frac{Uf\delta_x}{\delta_z^2 N_m^2}\ll1, \quad \text{(A17c,d)}$$

where N_m^2 is the minimum value of N^2, U is a characteristic velocity scale, and $\delta_z\approx H$ is a typical z scale. We assume that typical values are $U\approx20$ cm s^{-1}, $\delta_x\approx15$ km, $\delta_y\approx1000$ km, $\delta_z\approx100$ m, $N\approx10^{-2}$ s^{-1}, $f\approx10^{-4}$ s^{-1}, $\delta_t\approx14$ days, which gives $R_1\approx0.13$, $R_2\approx0.04$, $R_3\approx0.2$ and $R_4\approx0.3$. These values are reasonably small and we will proceed and ignore the effect of the basic current and use (A4).

We next consider the barotropic problem. In order to point out some qualitative features of the barotropic response we will simplify the problem and assume that the bottom topography of the shelf and slope is given by (Buchwald and Adams, 1968)

$$H=H_0\exp(-x/\delta_B), \quad \text{(A18)}$$

for $-L\leqslant x\leqslant0$, and that H does not vary with y. At $x=-L$ the slope adjoins a flat-bottomed ocean interior with a constant depth, $H=H_0\exp(L/\delta_B)$. We follow

a procedure somewhat similar to that of Gill and Schumann (1974).

For the barotropic component we may assume that the governing equations are

$$u_x+v_y+w_z=0, \quad \text{(A19a)}$$

$$-fv=-p_x/\rho_0, \quad \text{(A19b)}$$

$$v_t+fu=-p_y/\rho_0, \quad \text{(A19c)}$$

$$0=-p_z, \quad \text{(A19d)}$$

where (A19b) again follows from (A1) and is equivalent to making a long-shelf-wave approximation. A transport streamfunction ψ may be defined, such that

$$Hu=\psi_y, \quad Hv=-\psi_x, \quad \text{(A20a, b)}$$

and (A19) may be combined into one equation for ψ, which is

$$(\psi_{xx}+\delta_B^{-1}\psi_x)_t-\delta_B^{-1}f\psi_y=0, \quad \text{(A21)}$$

where $\delta_B^{-1}=-H_x/H$. The boundary conditions for ψ are

$$\psi_y=-\tau_W/\rho_0 f, \quad x=0, \quad \text{(A22a)}$$

$$\psi_x=0, \quad x=-L, \quad \text{(A22b)}$$

where (A22b) follows from assumption (A1a) (Gill and Schumann, 1974). It is convenient to let

$$\tilde{\psi}_y=\psi_y+\tau_W/(\rho_0 f), \quad \text{(A23a)}$$

or

$$\tilde{\psi}=\psi-(\rho_0 f)^{-1}\int_{-\infty}^{y}\tau_W(\bar{y},t)d\bar{y}, \quad \text{(A23b)}$$

and to solve for $\tilde{\psi}$. The term $\tau_W/(\rho_0 f)$ in (A23a) just represents a u component which balances two-dimensionally, i.e., in a plane normal to the coast, the suction into the surface Ekman layer at $x=0$ (A22a). With the substitution of (A23), Eqs. (A21) and (A22) become

$$(\tilde{\psi}_{xx}+\delta_B^{-1}\tilde{\psi}_x)_t-\delta_B^{-1}f\tilde{\psi}_y=-\tau_W(\rho_0\delta_B)^{-1}, \quad \text{(A24)}$$

$$\tilde{\psi}_y=0, \quad x=0, \quad \text{(A25a)}$$

$$\tilde{\psi}_x=0, \quad x=-L. \quad \text{(A25b)}$$

The problem now is identical in form to that treated by Gill and Schumann (1974). $\tilde{\psi}$ may be expanded in terms of the free-shelf-wave eigenfunctions $F_n(x)$, i.e.,

$$\tilde{\psi}=\sum_n G_n(y,t)F_n(x), \quad \text{(A26)}$$

where F_n satisfies the eigenvalue problem

$$F_{nxx}+\delta_B^{-1}F_{nx}+\beta_n^2 F_n=0, \quad \text{(A27a)}$$

$$F_n=0, \quad x=0, \quad \text{(A27b)}$$

$$F_{nx}=0, \quad x=-L. \quad \text{(A27c)}$$

The solution for F_n is

$$F_n=\exp(-\tfrac{1}{2}x/\delta_B)\sin(k_nx/L), \quad \text{(A28a)}$$

where k_n $(n=1, 2, 3, \ldots)$ is the nth root of

$$\tan k_n = -2\delta_B k_n/L, \tag{A28b}$$

and

$$\beta_n^2 = (k_n/L)^2 + \tfrac{1}{4}\delta_B^{-2}. \tag{A28c}$$

Expanding

$$1 = \sum_n b_n F_n(x), \tag{A29}$$

and substituting (A26) and (A29) into (A24), we find that G_n satisfies the forced first-order wave equation

$$a_n^{-1}G_{nt} + G_{ny} = \tau_W b_n (f\rho_0)^{-1}, \tag{A30}$$

where

$$a_n = f/(\delta_B \beta_n^2) \tag{A31}$$

is the phase velocity of free, long shelf waves. We note that the derivation of an equation of the form (A30) does not depend on the simplified exponential bottom topography and that a similar result will follow for more general $H = H(x)$ (Gill and Schumann, 1974).

To account for frictional effects, Gill and Schumann (1974) suggest the modification of (A30) to, essentially,

$$a_n^{-1}G_{nt} + G_{ny} + (a_n T_F)^{-1}G_n = \tau_W b_n (f\rho_0)^{-1}, \tag{A32}$$

where T_F is a frictional time scale. Allen (1975b) has examined the effect of bottom friction, through Ekman layer pumping, on forced coastal trapped waves. For barotropic shelf waves, (A32) is a reasonable model. The frictional effect is not so simple, however, for forced internal Kelvin waves and the simple addition of a frictional term is not appropriate for (A11).

Some properties of the solutions of (A30) and (A11) are referred to in Section 8 in relation to the observations. For that purpose, a few solutions with simple expressions for the wind stress τ_W are given here.

If the wind stress τ_W is independent of y, or if it may be locally regarded as such, then $\bar{\psi}_y \equiv 0$ and (A24) may be easily solved directly. For example, consider that the wind stress is

$$\tau_W = \tau_{W0} e^{i\omega t}, \tag{A33}$$

where τ_{W0} is a constant. Then the solution to (A24) is

$$Hv = -\bar{\psi}_x = \tau_{W0}(\omega\rho_0)^{-1}e^{i(\omega t - \pi/2)}$$
$$\times \{1 - \exp[-(x+L)/\delta_B]\}, \tag{A34a}$$

where

$$Hu = \psi_y = -\tau_{W0}(f\rho_0)^{-1}e^{i\omega t}. \tag{A34b}$$

In this case, the time variation of u is π radians out of phase with the wind stress and v lags τ_W by $\tfrac{1}{2}\pi$. This result, of course, is consistent with the balance $v_t + fu = 0$ in (A19c).

Let us now consider the solution to (A30) when τ_W has the simple form of a traveling wave, i.e., for

$$\tau_W = \tau_{W0} \cos(\omega t + ly), \tag{A35}$$

where we assume, for convenience, that $\omega \geqslant 0$. From (A30), we obtain

$$G_n = \frac{b_n \tau_{W0} \sin(\omega t + ly)}{f\rho_0(a_n^{-1}\omega + l)}. \tag{A36}$$

For simplicity, we concentrate on the first mode, $n=1$, and on its contribution to u and v, which we denote by $u_{(1)}$ and $v_{(1)}$. From (A20), (A23) and (A26) we obtain

$$Hu_{(1)} = G_{1y}F_1, \tag{A37a}$$

$$Hv_{(1)} = -G_1 F_{1x}. \tag{A37b}$$

From (A28a) we find that $F_1 \leqslant 0$ and $F_{1x} \geqslant 0$ for $-L \leqslant x \leqslant 0$ and also from (A27)–(A29) that $b_1 \leqslant 0$. It follows that

$$Hu_{(1)} = \frac{|b_1|\tau_{W0}l}{f\rho_0(a_1^{-1}\omega + l)} \cos(\omega t + ly)|F_1|, \tag{A38a}$$

$$Hv_{(1)} = \frac{|b_1|\tau_{W0}}{f\rho_0(a_1^{-1}\omega + l)} \cos[(\omega t + ly) - \tfrac{1}{2}\pi]|F_{1x}|. \tag{A38b}$$

Recall that the expression for the total u velocity component (A23a) is

$$Hu = \sum_n Hu_{(n)} + Hu_S, \tag{A39a}$$

where

$$Hu_S = -(f\rho_0)^{-1}\tau_W. \tag{A39b}$$

Considering only the contribution from the first mode and Hu_S, i.e.,

$$Hu = Hu_{(1)} + Hu_S + \cdots, \tag{A40}$$

we obtain

$$Hu = -\frac{\tau_{W0}}{f\rho_0} \cos(\omega t + ly)\left[1 - \frac{|b_1||F_1|l}{(a_1^{-1}\omega + l)}\right] + \cdots. \tag{A41}$$

From (A38b) and (A41) we see that, at a fixed value of y, the time variation of u may be either in phase or π radians out of phase with the wind stress and that, if $(a_1^{-1}\omega + l) > 0$, $v_{(1)}$ lags τ_W by $\tfrac{1}{2}\pi$, whereas if $(a_1^{-1}\omega + l) < 0$, $v_{(1)}$ leads τ_W by $\tfrac{1}{2}\pi$. Note that, for $l=0$, the phase results of (A34) are recovered.

For $(a_1^{-1}\omega + l) = 0$, there is a resonance condition and the solution for G_1, which satisfies $G_1(t=0) = 0$, is

$$G_1 = a_1 b_1 (f\rho_0)^{-1}\tau_{W0}t \cos(\omega t - |l|y). \tag{A42}$$

We then obtain

$$Hu_{(1)} = -a_1 b_1 (f\rho_0)^{-1}\tau_{W0}t \cos(\omega t - |l|y - \pi/2)|F_1|l|, \tag{A43a}$$

$$Hv_{(1)} = a_1 b_1 (f\rho_0)^{-1}\tau_{W0}t \cos(\omega t - |l|y)|F_{1x}|. \tag{A43b}$$

As far as the time oscillating part is concerned, $v_{(1)}$ is in phase with the wind stress τ_W and $u_{(1)}$ lags $v_{(1)}$ and τ_W by $\tfrac{1}{2}\pi$.

Dissipative effects will, of course, limit the growth of the resonant response. In fact, if (A32) is utilized, the directly forced solution for G_1, when $(\omega a_1^{-1} + l) = 0$, is

$$G_1 = a_1 b_1 T_F (f \rho_0)^{-1} \tau_{W0} \cos(\omega t - |l| y). \quad (A44)$$

It again follows that $v_{(1)}$ is in phase with τ_W and that $u_{(1)}$ lags $v_{(1)}$ by $\frac{1}{2}\pi$. If the resonant solution $u_{(1)}$ is greater in magnitude than u_S, then the phase behavior given in (A43a) should dominate, for $x < 0$, that from u_S.

If the wind stress is in the form of a standing wave, i.e., assuming $l \geqslant 0$, if

$$\tau_W = \tau_{W0} \cos ly \cos \omega t$$
$$= \frac{1}{2}\tau_{W0}[\cos(\omega t + ly) + \cos(\omega t - ly)], \quad (A45)$$

then the solution for G_1 is

$$G_1 = \frac{b_1 \tau_{W0}}{f \rho_0 (a_1^{-2}\omega^2 - l^2)}[a_1^{-1}\omega \cos ly \cos(\omega t - \frac{1}{2}\pi)$$
$$- l \sin ly \cos \omega t]. \quad (A46)$$

For $a_1^{-1}\omega \gg l$, corresponding to a balance between the first and third terms in (A30), i.e., to a two-dimensional $v_t + fu = 0$ balance in (A19c), we obtain

$$G_1 \approx b_1 \tau_{W0}(f \rho_0 a_1^{-1}\omega)^{-1} \cos ly \cos(\omega t - \frac{1}{2}\pi), \quad (A47a)$$

and

$$Hu_{(1)} = -|b_1|\tau_{W0}(f \rho_0 a_1^{-1}\omega)^{-1}l$$
$$\times \sin ly \cos(\omega t - \frac{1}{2}\pi)|F_1|, \quad (A47b)$$

$$Hv_{(1)} = |b_1|\tau_{W0}(f \rho_0 a_1^{-1}\omega)^{-1}$$
$$\times \cos ly \cos(\omega t - \frac{1}{2}\pi)|F_{1x}|. \quad (A47c)$$

Similar to the behavior in (A38b), $v_{(1)}$ lags τ_W in time by $\frac{1}{2}\pi$. In contrast to (A38a), however, here $u_{(1)}$ either lags τ_W by $\frac{1}{2}\pi$ or leads τ_W by $\frac{1}{2}\pi$ depending on the value of y.

For $a_1^{-1}\omega \ll l$, corresponding to a balance of the second and third terms in (A30), i.e., to a geostrophic balance in (A19c), we obtain

$$G_1 \approx b_1 \tau_{W0}(f \rho_0 l)^{-1} \sin ly \cos \omega t, \quad (A48a)$$

and

$$Hu_{(1)} = |b_1|\tau_{W0}(f \rho_0 l)^{-1} \cos ly \cos \omega t |F_1|, \quad (A48b)$$

$$Hv_{(1)} = |b_1|\tau_{W0}(f \rho_0 l)^{-1} \sin ly \cos \omega t |F_{1x}|. \quad (A48c)$$

In this case, the time variation of $u_{(1)}$ is in phase with τ_W and $v_{(1)}$ either is in phase or is π radians out of phase with τ_W, depending on the value of y.

For $a_1^{-1}\omega = l$, there is a resonance condition due to the northward traveling component of the standing wave in (A45). Again, the resonant response should dominate.

We have summarized these results on the time phase relation of $v_{(1)}$, $u_{(1)}$ and u_S with τ_W in Table 8. Similar results will hold for the higher modes $v_{(n)}$ and $u_{(n)}$, except that there may be changes in phase of π due to

changes in sign, for different values of x, in F_n and F_{nx}. The addition of frictional effects, e.g., through (A32), will lead to additional phase changes, but we do not explore these here, except to note that the phase relations for the resonance cases, as defined in reference to (A43) and the frictional solution (A44), are the same.

The alongshore and time, i.e., y and t, behavior of the baroclinic modes is governed by a similar forced first-order wave equation (A11). One difference in the interpretation of the solutions to that equation for the baroclinic mode, however, is that the total baroclinic u component is given by

$$u = \sum_n u_n = -(\rho_0 f)^{-1} \sum_n \tau_{Wn} X_n Z_n, \quad (A49)$$

and u is, consequently, directly determined by τ_{Wn}. Since $\tau_{Wn} = d_n \tau_W$, where d_n is a constant whose sign depends on n, u_n is always either in phase or 180° out of phase with τ_W [e.g., with the signs defined as in Section 5 such that $Z_2(0) < 0$, then $d_2 > 0$, and u_2 is 180° out of phase with τ_W]. On the other hand, the baroclinic v component is given by

$$v = \sum_n v_n = (\rho_0 f)^{-1} \sum_n Y_n X_{nx} Z_n, \quad (A50)$$

and v_n is determined by Y_n. Since this is similar to the way in which the barotropic $v_{(n)}$ is related to G_n, the conclusions, from the previous examples on the relation of the barotropic component of v with the wind stress (Table 8), will hold in a similar way for the baroclinic v components.

APPENDIX B

Empirical Orthogonal Decomposition

To understand the meaning of the empirical orthogonal functions used in Section 6, consider an ensemble of sample functions $\{v(z)\}$, a single realization of which can be denoted by $v_k(z)$. Assuming ergodicity, the index k could be regarded here as time t_k ($k = 1, 2, \ldots, K$). Also, in the present context the functions are defined at a finite number of values of z_i, $i = 1, \ldots, N$. To fix ideas, the quantity $v_k(z_i)$ could be regarded as the velocity at depth z_i at time t_k. Imagine that for each time t_k the data $v_k(z_i)$, $i = 1, \ldots, N$, are plotted as a point or a vector in an N-dimensional space; there are therefore K points in this space.

We shall interpret the empirical eigenfunctions as the principal directions or axes of these data points in this N dimensional space. Their physical significance is identical to the principal directions of solids or stress fields. We consider the case of solids, where one defines a moment of inertia tensor with respect to certain Cartesian axes as

$$I_{ij} = \int x_i x_j dv, \quad (B1)$$

where x_i is the position of a volume element dv, and the integral is carried out over the entire volume of the solid. To locate the principal direction of this solid, one tries to find the axes which diagonalize the matrix I_{ij}. Then the "normal" moment of inertia (diagonal term) is maximized along one axis and is minimized along another axis. The third axis is another stationary direction along which a slight change of direction decreases the magnitude of the inertia.

In the present case, the quantity analogous to the inertia tensor in (B1) is obviously the real and symmetric matrix of correlation coefficients

$$R(z_i, z_j) = \frac{1}{K} \sum_{k=1}^{K} v_k(z_i) v_k(z_j), \quad (B2)$$

where the sum over time takes the place of volume integration in (B1). If a new set of orthogonal "axes" $\phi_n(z_i)$, defined by

$$\sum_{i=1}^{N} R(z_i, z_j) \phi_n(z_i) = \lambda_n \phi_n(z_j), \quad n = 1, \cdots, N, \quad (B3)$$

i.e., by the eigenvectors of the correlation matrix, are chosen and one defines new variables E_{kn} referred to the new axes

$$E_{kn} = \sum_{i=1}^{N} v_k(z_i) \phi_n(z_i), \quad (B4)$$

then the new correlation matrix does not have off-diagonal terms; i.e.,

$$\frac{1}{K} \sum_{k=1}^{K} E_{kn} E_{km} = \lambda_n \delta_{nm}. \quad (B5)$$

From this it follows that

$$\frac{1}{K} \sum_{k=1}^{K} E_{kn}^2 = \lambda_n, \quad (B6)$$

so that the eigenvalues are the mean-square values of the coefficients, that is, the average energy in the various modes. It is easy to show that the sum of the eigenvalues add up to the total energy:

$$\frac{1}{K} \sum_{k=1}^{K} \sum_{i=1}^{N} v_k^2(z_i) = \frac{1}{K} \sum_{k=1}^{K} \sum_{n=1}^{N} E_{kn}^2 = \sum_{n=1}^{N} \lambda_n. \quad (B7)$$

It is well known that when a real and symmetric matrix is diagonalized, one of the diagonal terms is maximized, another is minimized, and the remaining also reach stationary values. It is therefore clear that along any orthogonal principal direction the sum of the squares of the projections of all the data vectors in the N-dimensional space is extremized. If the eigenvalues are arranged such that $\lambda_1 > \lambda_2 > \cdots \lambda_N$, then the eigenvector ϕ_1 is the "best direction"[4] (maximum projection),

---

[4] ϕ_1 is really the straight-line fit to the data in the N space, minimizing the least-square normal error.

ϕ_N is the "worst direction," and the others are simply stationary directions for which a slight change of direction decreases the magnitude of the projection, with the plane formed by ϕ_1-ϕ_2 being the "best plane" etc.

From this discussion it is also intuitively obvious that ϕ_1 extracts the maximum energy out of the ensemble, ϕ_2 extracts the maximum energy out of what is left, and so on. [For a rigorous proof, see Busch and Peterson (1971).] This leads to the conclusion that the expansion of the sample function in terms of the empirical eigenfunctions ϕ_n is the one which leads to the *fastest convergence* of the series. Hence, only a few terms are needed to account for most of the variance of the ensemble.

The connection of the empirical and dynamic mode shapes should also be mentioned. It can be noted that if eigenfunctions obey the orthogonality relation (6.3) and their amplitudes obey the time uncorrelation relation (B5), then the eigenfunctions must obey relation (B3); that is, (B3) follows if (6.3) and (B5) hold. If the vertical resolution of the data series is high enough and the vertical span complete so that integrals can be replaced by sums, (5.6) would be approximated by a relation like (6.3), and if the dynamics of the ocean is such that the amplitudes of the various modes are uncorrelated in time, then from the above discussion it follows that the dynamic modes Z_n would roughly obey a relation like (B3) and the empirical and dynamic modes would be similar in shape. However, if the dynamics is such that the amplitudes are correlated in time, as is predicted, for example, from simple upwelling theories where the wind stress directly drives both the barotropic and baroclinic modes, then the empirical modes will be linear combinations of the dynamic modes.

REFERENCES

Allen, J. S., 1973: Upwelling and coastal jets in a continuously stratified ocean. *J. Phys. Oceanogr.*, 3, 245–257.

——, 1975a: Coastal trapped waves in a stratified ocean. *J. Phys. Oceanogr.*, 5, 300–325.

——, 1975b: The effect of bottom friction on the forced wave response of stratified coastal regions (in preparation).

Buchwald, V. T., and J. L. Adams, 1968: The propagation of continental shelf waves. *Proc. Roy. Soc. London*, A305, 235–250.

Busch, N. E., and E. L. Petersen, 1971: Analysis of nonstationary ensembles. *Statistical Methods and Instrumentation in Geophysics*, A. S. Kjelaas, Ed., Proceedings of the NATO Advanced Study Institute in Norway, April 1971, Teknologisk Forlag, Oslo.

Cutchin, D. L., and R. L. Smith, 1973: Continental shelf waves: Low frequency variations in sea level and currents over the Oregon continental shelf. *J. Phys. Oceanogr.*, 3, 73–82.

Gill, A. E., and A. J. Clarke, 1974: Wind-induced upwelling, coastal currents and sea-level changes. *Deep-Sea Res.*, 21, 325–345.

——, and E. H. Schumann, 1974: The generation of long shelf waves by the wind. *J. Phys. Oceanogr.*, 4, 83–90.

Halpern, D., and J. R. Holbrook, 1972: STD measurements off the Oregon coast during July/August 1972. CUEA Data Report 4.

Holbrook, J. R., and D. Halpern, 1974: STD measurements off the Oregon coast during July/August 1973. CUEA Data Report 12.

Huyer, A., R. L. Smith and R. D. Pillsbury, 1974: Observations in a coastal upwelling region during a period of variable winds (Oregon coast, July 1972). *Tethys*, 6, 391–404.

Kosambi, D. D., 1943: Statistics in function space. *J. Indian Math. Soc.*, 7, 76–88.

Kundu, P. K., and J. S. Allen, 1975: Some three-dimensional characteristics of low frequency current fluctuations near the Oregon coast. (Submitted to *J. Phys. Oceanogr.*)

Lumley, J. L., 1970: *Stochastic Tools in Turbulence*. Academic Press, 194 pp.

Mooers, C. N. K., and J. S. Allen, 1973: Final Report of the CUEA Summer 1973 Theoretical Workshop. School of Oceanography, Oregon State University.

——, C. A. Collins and R. L. Smith, 1972: The dynamic structure of the frontal zone in the coastal upwelling region off Oregon. (Submitted to *J. Phys. Oceanogr.*)

Mysak, L. A., 1967: On the theory of continental shelf waves. *J. Marine Res.*, 25, 205–227.

Pedlosky, J., 1974: Longshore currents and the onset of upwelling over bottom slope. *J. Phys. Oceanogr.*, 4, 310–320.

Pillsbury, R. D., J. S. Bottero, R. E. Still and W. E. Gilbert, 1974: A compilation of observations from moored current meters. Vols. VI and VII, Refs. 74-2 and 74-7, School of Oceanography, Oregon State University.

Robinson, A. R., 1964: Continental shelf waves and the response of sea level to weather systems. *J. Geophys. Res.*, 69, 367–368.

Smith, R. L., 1974: A description of the current, wind, and sea level variations during coastal upwelling off the Oregon coast, July–August 1972. *J. Geophys. Res.*, 79, 435–443.

Walin, G., 1972: On the hydrographic response to transient meteorological disturbances. *Tellus*, 24, 169–186.